

Measurement report: Contribution of atmospheric new particle formation to ultrafine particle concentration, cloud condensation nuclei and radiative forcing: Results from five-year observations in Central Europe

5 Jia Sun^{1,2}, Markus Hermann², Kay Weinhold², Maik Merkel², Wolfram Birmili³, Yifan Yang², Thomas Tuch², Harald Flentje⁴, Björn Briel⁴, Ludwig Ries³, Cedric Couret³, Michael Elsasser³, Ralf Sohmer³, Klaus Wirtz³, Frank Meinhardt³, Maik Schütze³, Olaf Bath³, Bryan Hellack³, Veli-Matti Kerminen⁵, Markku Kulmala⁵, Nan Ma⁶, Alfred Wiedensohler²

¹Southern Marine Science and Engineering Guangdong Laboratory (Guangzhou), Guangzhou, China

10 ²Leibniz Institute for Tropospheric Research (TROPOS), Leipzig, Germany

³German Environment Agency (UBA), Berlin, Germany

⁴Deutscher Wetterdienst (DWD), Meteorologisches Observatorium Hohenpeißenberg, Germany

⁵Department of Physics, University of Helsinki, P.O. Box 64, 00014 Helsinki, Finland

⁶Institute for Environmental and Climate Research, Jinan University, Guangzhou, Guangdong 511443, China

15

Correspondence to: Nan Ma (nan.ma@jnu.edu.cn) and Alfred Wiedensohler (ali@tropos.de)

Abstract. As an important source of sub-micrometer particles, atmospheric new particle formation (NPF) has been observed in various environments. However, most studies provide little more than snapshots of the NPF process due to their underlying observations being limited in space and time. To obtain statistically relevant evidence on NPF across various environments, we investigated the characteristics of NPF based on a five-year dataset of the German Ultrafine Aerosol Network (GUAN). The results were also compared with the observations in previous studies, aiming to depict a relatively complete picture of NPF in Central Europe. The highest NPF occurrence frequency was observed in regional background, with an average of about 19 %, followed by urban background (15 %), low mountain range (7 %) and high Alpine (3 %). The annual mean growth rate between 10 and 25 nm varied from 3.7 to 4.7 nm h⁻¹, while the formation rate with same size range 10–25 nm from 0.4 to 2.9 cm⁻³ s⁻¹. The contribution of NPF on UFPs was about 13 %, 21 %, and 7% for the urban background, regional background, and low mountain range, respectively. The influence of NPF on CCN number concentration and aerosol extinction coefficient for NPF days were the highest in mountainous area. These findings underscore the importance of the local environments when assessing the potential impact of NPF on regional climate in models, and also emphasize the usefulness of a long-term aerosol measurement network for understanding the variation of NPF features and their influencing factors over a regional scale.

20

25

30 **1 Introduction**

Atmospheric new particle formation (NPF) is a process initiated with the sudden formation of new particles with diameters less than 3 nm in the atmosphere. Low volatile gas molecules oxidated from gas-phase precursors cluster together and form new aerosol particles. These nano particles may subsequently grow into larger sizes by condensation or coagulation (Kulmala et al., 2014). The newly formed aerosol particles have the potential to contribute greatly to the number concentration of
35 ultrafine particles (UFPs, particles smaller than 100 nm) or even larger sub-micrometer particles (particles smaller than 1 μm) (Ma and Birmili, 2015). Once the newly formed particles grow into larger sizes (typically more than 100 nm), they can affect cloud properties and processes by acting as cloud condensation nuclei (CCN) (Dameto De España et al., 2017; Hirshorn et al., 2022; Ren et al., 2021; Williamson et al., 2019). As an essential source of atmospheric aerosols, NPF events can also impact the regional radiative forcing of the atmosphere by increasing the overall extinction of light as the particles grow larger (Shen
40 et al., 2011).

NPF is a complex process affected by various factors, including meteorological conditions (Bousiotis et al., 2021a; Li et al., 2019; Salvador et al., 2021), atmospheric chemical composition (Dada et al., 2020; Dall'Osto et al., 2018; Németh et al., 2018; Nieminen et al., 2014), and pre-existing aerosol loading (Bousiotis et al., 2021b; Salma and Németh, 2019), etc. Studies on NPF have been conducted in diverse environments, ranging from polluted megacity (Yao et al., 2018; Wang et al., 2014)
45 to clean areas (Petäjä et al., 2009; Vana et al., 2016). Experimental observations show that in the continental boundary layer, NPF often occurs in the shape of “NPF events”, i.e., the nucleation and subsequent growth of particles may take place over horizontal spatial scales up to several tens or hundreds of kilometers. Such “banana” type NPF events with particle formation and growth can accordingly occur across various locations and diverse types of environments (Kerminen et al., 2018). The basis of experimental observations has grown steadily over the past 30 years, and a plethora of computational models have
50 been developed to describe NPF on mechanistic and empirical levels.

However, the conclusions drawn from existing studies show large discrepancies, and the influence of local atmospheric or meteorological conditions on NPF has not been fully understood yet. For instance, although some studies reported that low ambient relative humidity (RH) environments favour NPF (Cai et al., 2017; Dada et al., 2017; Li et al., 2019), NPF has still been observed in the environments with high RH (O'Dowd et al., 1998; Bousiotis et al., 2021b). High temperature associated
55 with strong solar radiation can promote photochemical reaction and nucleation (Boy and Kulmala, 2002; Kürten et al., 2016; Ma and Birmili, 2015) and a well-mixed air leads to low condensational sink (CS), resulting in a higher probability for NPF (Größ et al., 2018; Dall'Osto et al., 2018; Bousiotis et al., 2021a). Conversely, high temperature and a well-mixed atmosphere may also inhibit NPF by decreasing the stability of molecular clusters (Hanson et al., 2017; Kürten et al., 2018). Additionally, the role of mixed atmospheric chemical species, including SO_2 , NH_3 , and volatile organic compounds (VOCs), is complex and
60 varies with the nucleation mechanism and concentration of those components (Laaksonen et al., 2008; Ehn et al., 2014; Kürten et al., 2016; Qi et al., 2018). To understand the characteristics of NPF and its influencing factors, field campaign experiments covering a wide range of atmospheric conditions and environments are essential (Lee et al., 2019).

Continuous observations of NPF started as single point observations at ground level (Mäkelä et al., 1997; Birmili and Wiedensohler, 2000), and were subsequently expanded to cover greater spatial and temporal scales. Several studies have investigated NPF at multiple sites at small-region-scale (for example around a city) (Costabile et al., 2009; Németh and Salma, 2014; Bousiotis et al., 2019; Casquero-Vera et al., 2020; Kalkavouras et al., 2020; Smejkalova et al., 2021; etc.), at country- or continent-scale (Manninen et al., 2010; Dall'Osto et al., 2018; Németh et al., 2018; Bousiotis et al., 2021a; Sebastian et al., 2022; etc.), and at global-scale (Ren et al., 2021; Nieminen et al., 2018; Sellegri et al., 2019). Small-region-scale studies refer to individual NPF observations within regional and closer distance (< 200 km), such as in central France (Boulon et al., 2011), Budapest (Németh and Salma, 2014; Salma et al., 2017), southern UK (Bousiotis et al., 2019), and Leipzig (Ma and Birmili, 2015). These studies mainly focused on the difference in NPF features with varied degree of anthropogenic and biogenic emissions (Ma and Birmili, 2015; Bousiotis et al., 2019), or the characteristics of NPF events occurring simultaneously at several sites in a small area (Németh and Salma, 2014; Salma et al., 2016). Country-based or continental-scale studies can provide insight into the connection between NPF events and their influencing factors covering a particular region, such as Europe (Dall'Osto et al., 2018; Bousiotis et al., 2021b; Manninen et al., 2010) and India (Sebastian et al., 2022). Global analyses of NPF events stretch these comparisons further, comparing the characteristics of NPF under one (Sellegri et al., 2019) or multiple types of environments (Nieminen et al., 2018; Ren et al., 2021). However, comprehensive observations of regional NPF across multiple sites have still been limited to date, with most studies including only 2 or 3 sites, leading to open questions when explaining the spatial and temporal variabilities of regional NPF across diverse environments throughout a large region.

The German Ultrafine Aerosol Network (GUAN) is an observation network for sub-micrometer aerosol particles measurements, aiming at a better understanding of the associated climate and health effects. GUAN provides long-term atmospheric aerosol measurements in diverse site categories in Germany, ranging from roadside to high Alpine area (Birmili et al., 2016; Sun et al., 2020). On the basis of the GUAN observations, a comprehensive comparison of NPF in various environments across Germany becomes realistic. Based on a five-year dataset we investigated the characteristics of NPF for various environments from urban background to high Alpine, including the occurrence of NPF events, particle formation and growth rates, and the impacts of NPF on UFP, CCN and radiative forcing, aiming to depict a relatively complete picture of NPF in Central Europe.

2 Measurement and data

2.1 Measurement sites

This study uses atmospheric observations from nine observation sites in the German Ultrafine Aerosol Network (GUAN; Birmili et al., 2016; <https://doi.org/10.5072/guan>, last access: 30 August 2023). GUAN is a cooperative observation network of several research organizations providing continuous measurement of sub-micrometer particle number size distributions (PNSD) and equivalent black carbon (eBC) mass concentration since 2009. GUAN consists of 17 measurement sites covering diverse environmental settings in Germany including roadside, urban background, regional background, low mountain range

95 and high Alpine. The locations and characteristics of the nine selected measurement sites are shown in Fig.1 and Table 1. For a detailed description, see Birmili et al. (2016).

The nine GUAN measurement sites in this study comprise three urban background sites, three regional background sites, two low mountain range sites and one high Alpine site. Three urban background sites are Leipzig-West (LWE), Leibniz Institute for Tropospheric Research (TROPOS) (LTR), and Bösel (BOS). LWE and LTR are both located in the city of Leipzig
100 with 10 km apart. LTR is situated on the roof of the TROPOS main building, while LWE is settled in a hospital park in the western suburbs of Leipzig. BOS is located in the village of Bösel, about 100 km away from the North Sea.

The regional background site Melpitz (MEL) is distant about 50 km in the north-east of Leipzig. Its surroundings of MEL are flat and seminatural grasslands without significant anthropogenic sources. Site Neuglobsow (NEU) and Waldhof (WAL) are situated in Northern Germany forest regions. One previous study showed that MEL can represent the regional background
105 atmosphere of Central Europe (Spindler et al., 2013), while NEU and WAL represent the regional background condition in the northern Germany lowlands (Sun et al., 2019).

Three mountainous sites in GUAN are located in the southern Germany, including two low mountain range sites Schauinsland (SCH, 1205 m a.s.l.) and Hohenpeißenberg (HPB, 980 m a.s.l.), and one high Alpine site Zugspitze-Schneefernerhaus (ZSF, 2670 m a.s.l.). SCH is situated in the Black Forest and HPB is on a solitary hill in the countryside of
110 southern Bavaria, 40 km north of the Alpine Mountain range and 45 km southwest of Munich region. As a part of the World Meteorological Organisation (WMO) Global Atmosphere Watch (GAW) program, ZSF is located on the south side of Zugspitze Mountain approximately 300 m below the summit and the airmasses of both lower free troposphere (FT) and planetary boundary layer (PBL) can be observed there (Sun et al., 2021; Yuan et al., 2019).

2.2 Instrumentation

115 Aerosol PNSDs were measured by either Mobility Particle Size Spectrometers (MPSS, Wiedensohler et al., 2012), dual mobility particle size spectrometers (D-MPSS). Some stations used an additional thermodenuder option, Thermodenuder Mobility Particle Size Spectrometers (TDMPSS, Wang et al., 2017), whose data, however, were not used in this analysis. The specifications of the instruments used at each site are summarized in Table 1. To ensure standardized conditions for particle sizing at different sites and times, PNSDs were generally measured in a dry state with RH below 40 % (Swietlicki et al., 2008).
120 An inversion algorithm developed by Pfeifer et al. (2014) based on bipolar charge distribution (Wiedensohler, 1988) was used to retrieve the PNSD from the measured raw mobility distribution. The particle losses in instruments and inlet systems were corrected based on Wiedensohler et al. (2012) and the quality assurances (QAs) were done as described in Wiedensohler et al. (2018).

The QA of MPSS measurements in GUAN, including both instrument to instrument and instrument to standard
125 comparisons, was regularly conducted by the World Calibration Centre for Aerosol Physics (WCCAP, <http://www.wmo-gaw-wcc-aerosol-physics.org/>, last access:12 April 2023) in Leipzig. The aim of QA is to obtain an accuracy within a few percent for the particle sizing and ± 10 % for particle number concentration (PNC) of PNSD over the entire measurement period. The

periodical QA procedures for MPSS includes daily or weekly inspection, monthly and annual full maintenance, either at measurement site or at laboratory of WCCAP. Detailed descriptions of the QA procedure are given in Birmili et al. (2016).

130 The PNSD data used in this study covers a five-year period from 2009 to 2013, with three exceptions: NEU and LWE started PNSD measurements in 2011 and the PNSD data at ZSF are available from 2012. The temporal coverages of qualified PNSD data at the nine sites are given in Fig.S1 in the supplementary material.

2.3 Method

2.3.1 NPF events classification

135 The classification of NPF events was performed visually according to the criteria given by Dal Maso et al. (2005). If a distinct new nucleation mode (3–25 nm) appeared and grew into the Aitken mode size range (25–100 nm) within the subsequent hours between 00:00 and 24:00 local time, such a day was classified as a NPF day. The NPF event was classified as type I if the formation and growth rate of the NPF event could be clearly determined from the observed evolution of the PNSD, and type II if not. The formation and growth rates were calculated only for type I events. Type I events were further grouped into two sub-class: Ia and Ib. Class Ia contains very strong and clear NPF with “banana shape”. And the rest of type I events were classified as class Ib. The days were classified as “undefined event” if the cases could not be clearly classified as event or non-event.

2.3.2 Calculation of growth, formation rates and condensation sink

The growth and formation rate were evaluated for class I event in this study, while CS for all NPF events. The growth rate of nucleation mode particles (GR_{10-25}) is defined as the change rate of the modal diameter of the newly formed particles (Kulmala et al., 2012):

$$GR_{10-25} = \frac{(D_{P_2} - D_{P_1})}{(t_2 - t_1)}, \quad (1)$$

where D_{P_1} and D_{P_2} are the geometric mean diameters (GMDs) of the mode of newly formed particles at starting and ending time during a NPF event. The GMDs were obtained by the log-normal modal fitting of the PNSD.

150 The formation rate in nucleation mode (J_{10-25}) is the sum of the increase rate, decrease rate of N_{10-25} due to coagulation losses, and decrease rate of N_{10-25} due to the condensational growth out of the nucleation mode. Accordingly, J_{10-25} was obtained using the following equation (Kulmala et al., 2012):

$$J_{10-25} = \frac{dN_{10-25}}{dt} + \text{CoagS}_{10nm} \times N_{10-25} + \frac{GR_{10-25}}{\Delta D_p} \times N_{10-25} \quad (2)$$

155 where CoagS_{10nm} is the coagulation sink of particles with diameter of 10 nm, which can be calculated using the method proposed by Kerminen et al. (2001):

$$\text{CoagS}_{10nm} = \sum_{D_p'=10nm}^{D_p'=800nm} K(10nm, D_p') N_{D_p'} \quad (3)$$

where $K(10\text{nm}, D'_p)$ is the coagulation coefficient between particles with sizes of 10 nm and D'_p , and $N_{D'_p}$ is the particle number concentration of particle with size D'_p .

The condensation sink (CS) describes how fast the condensable vapour molecules condense on the pre-existing aerosol particles (Dal Maso et al., 2002), which can be obtained from

$$CS = 2\pi D \sum_i \beta_i d_{pi} N_i \quad (4)$$

where D is the diffusion coefficient of the vapour, calculated based on the properties of sulphuric acid. And d_{pi} is the diameter of a particle in size class i and N_i is the particle number concentration in the respective size class. β_i is the transition regime correction factor:

$$\beta_i = \frac{1+Kn}{1+\left(\frac{4}{3\alpha_i}+0.337\right)Kn+\frac{4}{3\alpha}Kn^2} \quad (5)$$

where α is the accommodation coefficient for mass transfer, which is assumed to be unity in our calculations. Kn is Knudsen number:

$$Kn = 6 \sqrt{\frac{\pi m}{8k_b T}} D \quad (6)$$

where m is the mass of a vapour molecule, T is temperature and k_b the Boltzmann constant.

170 2.3.3 Nucleation strength factor

The nucleation strength factor (NSF) proposed by Németh and Salma (2014) qualitatively evaluates the overall concentration increment on NPF days exclusively, calculated by:

$$NSF_{\text{nuc}} = \frac{(\frac{N_{10-100}}{N_{100-800}})_{\text{all NPF event days}}}{(\frac{N_{10-100}}{N_{100-800}})_{\text{all non-event days}}} \quad (7)$$

2.3.4 Contribution to UFP number concentration

175 The contribution of NPF on UFP number concentration was quantitatively estimated by segregating the diurnal patterns of UFP driven by NPF, urban sources and regional background (Ma and Birmili, 2015). As observed in the latter reference, NPF events occurred almost exclusively on days with a daily average solar radiation of more than 100 W m^{-2} in Germany. Subsequently, the measurement period was firstly separated into high and low solar radiation days by a threshold of daily average solar radiation 100 W m^{-2} , to accurately estimate the effect of NPF to UFP number concentration. The average diurnal cycles of

180 UFP number concentration for NPF days and non-event days at high solar radiation period were calculated and denoted as \tilde{N}_{HR-NPF} and \tilde{N}_{HR-NON} , respectively. Similarly, the corresponding values at low solar radiation period were calculated and denoted as \tilde{N}_{LR-NPF} and \tilde{N}_{LR-NON} . The average number concentration of newly formed particles for high and low radiation days were respectively calculated as:

$$\bar{N}_{NPF-HR} = \frac{\int_0^{24} (\tilde{N}_{HR-NPF} - \tilde{N}_{HR-NON}) \times dt}{24} \quad (8)$$

$$185 \quad \bar{N}_{\text{NPF-LR}} = \frac{\int_0^{24} (\bar{N}_{\text{LR-NPF}} - \bar{N}_{\text{LR-NON}}) \times dt}{24} \quad (9)$$

Accordingly, the overall contribution of NPF event to UFP concentration can be calculated as:

$$\bar{N}_{\text{NPF}} = \frac{\bar{N}_{\text{NPF-HR}} \times n_{\text{NPF-HR}} + \bar{N}_{\text{NPF-LR}} \times n_{\text{NPF-LR}}}{n_{\text{NPF-HR}} + n_{\text{NPF-LR}} + n_{\text{NON-HR}} + n_{\text{NON-LR}}} \quad (10)$$

where $n_{\text{NPF-HR}}$, $n_{\text{NPF-LR}}$, $n_{\text{NON-HR}}$, and $n_{\text{NON-LR}}$ are the number of days with high/low radiation and with/without NPF events, respectively.

190 2.3.5 Enhancement in CCN number concentration

The NPF-initiated enhancements in CCN number concentration (N_{CCN}) enhancement, denoted as $E_{N_{\text{CCN}}}$, was quantified using the method proposed by Ren et al. (2021) and Kalkavouras et al. (2019). This approach compares the N_{CCN} between after and prior to the NPF event:

$$E_{N_{\text{CCN}}} = \frac{N_{\text{CCN_after}}}{N_{\text{CCN_prior}}} \quad (11)$$

195 where $N_{\text{CCN_prior}}$ is the two-hour average of N_{CCN} before the start of NPF, and $N_{\text{CCN_after}}$ is determined as the average N_{CCN} during the period that NPF contributing on N_{CCN} . As a simplified estimate, N_{CCN} was calculated as the integral PNC with particle size larger than pre-defined critical diameter (D_c). Referring to a previous study by Wu et al. (2015), D_c of 50 nm, 70 nm and 180 nm were applied for 0.6, 0.4, and 0.1 % supersaturation, respectively. The start and end time of the period that NPF impacts on N_{CCN} were determined by evaluating the variability of normalized time series of N_{CCN} at each prescribed supersaturation.
 200 The detailed approach can be seen in Kalkavouras et al. (2019) and Ren et al. (2021). It should be noted that this method is based on the assumption that the background concentration of CCN holds constant during the NPF, ignoring the influence of other sources and sinks of aerosol particles, therefore it can only give a rough estimate of the impact of NPF on N_{CCN} .

2.3.6 Enhancement in extinction coefficient

The influence of NPF on radiative forcing was evaluated based on the measured PNSD and eBC mass concentration using the
 205 Mie theory. Assuming that BC is internal mixed and its volume fraction is independent of particles size, a uniform volume fraction of BC (VF_{BC}) for different particle sizes is defined as

$$VF_{\text{BC}} = \bar{V}_{\text{BC}} / \overline{PVC} \quad (12)$$

where, \bar{V}_{BC} , the mean volume concentration of BC particles is obtained by the mean eBC mass concentration during the observation period divided by the density of BC (1.5 g/cm³). \overline{PVC} is the average integral particle volume concentration (PVC)
 210 calculated from the measured PNSD.

Accordingly, the refractive index is derived as a volume-weighted average of BC and non-absorbing component:

$$\bar{m} = VF_{\text{BC}} \times \bar{m}_{\text{BC}} + (1 - VF_{\text{BC}}) \times \bar{m}_{\text{non-abs}} \quad (13)$$

where the refractive index for BC is set as $\bar{m}_{\text{BC}} = 1.96 - 0.66i$ (Seinfeld et al., 1998), and for non-absorbing component $\bar{m}_{\text{non-abs}} = 1.53 - 10^{-7}i$ (Wex et al., 2002).

215 The dimensionless extinction efficiency Q_{ext} can be obtained using Mie theory (Mie, 1908), and the extinction coefficient σ_{ext} can be calculated accordingly as:

$$\sigma_{\text{ext}} = \int_{D_p} Q_{\text{ext}} \times \left(\frac{\pi}{4} D_p^2\right) \times \text{PNSD} \times d\log D_p \quad (14)$$

Similar as the CCN enhancement estimation in Sect.2.3.5, the NPF-initiated enhancement of aerosol extinction coefficient (E_{ext}) was quantified as:

220 $E_{\text{ext}} = \sigma_{\text{ext_after}} / \sigma_{\text{ext_prior}} \quad (15)$

where, $\sigma_{\text{ext_prior}}$ is the two-hour average of σ_{ext} before the NPF start, and $\sigma_{\text{ext_after}}$ is determined as the average σ_{ext} during the period with NPF influence as described in Sect.2.3.5.

3 Results I: Basic features of NPF

3.1 NPF occurrence frequency

225 Table 2 presents the occurrence frequencies of NPF events observed at each site from 2009 to 2013, and the comparison of NPF occurrence frequency between GUAN sites and other European studies will be discussed in this section.

It should be noted that there are data missing for one to three years in four of the nine GUAN sites (Fig.S1). A question raised is whether the data missing may cause an issue of data representativeness. For UB sites, LTR and LWE had missing data in 2013 and 2009–2010, respectively. The sites LTR and LWE are both located in the city of Leipzig and are only 10 km
230 apart. As can be seen from Fig.S2, the NPF occurrence frequencies at the two sites were quite close during the overlapped period from June 2011 to 2012. Meanwhile, no significant inter-annual variation was found in the four-year data of LTR and three-year data of LWE. For RB sites, the observation at NEU was unavailable from 2009 to 2010. Both NEU and WAL can represent the regional background air in the northern Germany lowlands. And no significant inter-annual variation in NPF
235 occurrence frequency was found at WAL. Hence, we assume that the influence of the inter-annual changes on the characteristics of NPF in LTR, LWE and NEU are limited and the available dataset of these three sites can represent the overall characteristics of NPF for the five-year period. Among the three mountainous sites, ZSF had the least valid data, with only 2012 and 2013 available. The regional air mass occurrence frequency at ZSF increased slightly with a rate of 0.96 %/year from 2009 to 2013 (Sun et al., 2021), resulting in more frequent vertical transport of precursor gases to high-altitudes. The occurrence of NPF depends on several local conditions such as precursors concentration, condensation sink, temperature and
240 solar radiation, etc. However, the inter-annual variation of regional air mass occurrence frequency may imply that the characteristics of NPF at ZSF for 2012 and 2013 might be slightly biased with those for the whole period 2009–2013.

The NPF occurrence frequencies at the sites in the same category were found to be similar. The regional background sites had the highest NPF occurrence frequency, with an average of about 19 %, followed by the urban background sites with an average of about 15 %. NPF events were observed on about 7 % of days at low mountain range sites and only about 3 % of
245 days at the high Alpine site ZSF. A previous study by Nieminen et al. (2018) found similar annual and seasonal occurrence

frequencies for MEL and HPB. It is interesting that lower occurrence frequency of NPF is found at ZSF than the two low mountain range sites. The atmosphere in high altitude areas can be influenced by both PBL and FT (Sun et al., 2021; Herrmann et al., 2015; Rose et al., 2017). And NPF was found to be strongly associated with the air parcel vertically transported from lower altitudes (Bianchi et al., 2016; Shen et al., 2016; Tröstl et al., 2016). The influence of vertical transport of PBL air mass is much weaker at ZSF than lower altitudes, leading to lower condensation sink (CS) and concentrations of precursors. As reported in Flentje et al. (2010), the median SO₂ mass concentration during the year 2000–2007 at ZSF was about 0.18 µg/m³, which was lower than the one at HPB (0.31 µg/m³). Therefore, though the low temperature and CS at ZSF favour the NPF, the extremely low concentration of precursors at ZSF inhibits the occurrence of NPF, which is likely to be one of the possible reasons of the lower NPF occurrence frequency at ZSF.

Figure 2 compares the overall NPF occurrence frequencies at the GUAN sites with those of other sites in Europe (Baalbaki et al., 2021; Boulon et al., 2011; Bousiotis et al., 2019; Bousiotis et al., 2021b; Brines et al., 2015; Dameto De España et al., 2017; Herrmann et al., 2015; Hofman et al., 2016; Joutsensaari et al., 2018; Lee et al., 2020; Manninen et al., 2010; Németh et al., 2018; Nieminen et al., 2014; Plauskaite et al., 2010; Salma and Németh, 2019; Sellegri et al., 2019; Smejkalova et al., 2021; Vaananen et al., 2013; Vana et al., 2016). For detail information on the locations of those observation sites and study periods, please refer to Table S1 in the supplementary material.

The NPF occurrence frequencies at the three urban background sites in GUAN were found to be similar to those of other urban background sites in Central Europe, such as in Amsterdam (AMS), Budapest (BDP), and Vienna (VIE). The annual NPF occurrence frequencies at the three regional background sites in GUAN were at the medium range of all regional background sites, as illustrated in Fig.2. The highest NPF occurrence frequency was observed at the site Agia Marina Xyliatos (AMX) in Cyprus, with the occurrence frequency of 57 % and 8 % for NPF and undefined event, respectively. Generally, the site-to-site differences in NPF occurrence frequency are the result of many factors such as locations, meteorological conditions, and anthropogenic and biogenic emissions in the vicinity of the observation sites (Nieminen et al., 2018). For example, higher NPF occurrence frequency was observed at site AMX and CBW than MEL. One possible explanation is that both AMX and CBW are more affected by marine air masses (Manninen et al., 2010; Németh et al., 2018), while MEL is affected more by biogenic emissions from the surrounding forested areas (Bousiotis et al., 2021). When comparing the NPF occurrence frequency among different studies, the regional representativeness of individual observation site should be fully considered. Additionally, it needs to be careful when comparing those NPF features since the NPF event was visually classified. The subjective preference in the classification process may introduce bias in NPF occurrence frequencies. For instance, the occurrence frequencies of NPF events at mountain sites in GUAN were much lower than those of other mountain sites. Especially, the occurrence frequency of NPF was only 3.4 % at ZSF, while 14.5 % for another high Alpine site Jungfraujoch (JFJ) by Herrmann et al. (2015). In the visually classification process by Dal Maso et al. (2005), the potential NPF days can be classified as NPF event or undefined event. As stated by Herrmann et al. (2015), the occurrence frequencies of NPF event and undefined event are 14.5 % and 5.4 %, respectively for JFJ. The corresponding values are 3.3 % and 15.2 %, respectively for ZSF. This large

discrepancy in NPF occurrence frequency between these two sites may be resulted from the subjective decision when
280 classifying the dataset into NPF and undefined events during the visual classification process.

Figure 3 shows the monthly NPF occurrence frequencies of the nine GUAN sites, and the comparison of the seasonal
occurrence frequency of NPF between the nine GUAN sites and other European sites is illustrated in Fig.S2 in the
supplementary material. For most sites, the highest occurrence of NPF was found during spring and summer, while the lowest
in winter, which was consistent with the observations in the previous studies (e.g., Nieminen et al., 2018; Salma and Németh,
285 2019; Boulon et al., 2011). Such a seasonal pattern is highly related to the seasonal variations of solar radiation and biogenic
emissions (Manninen et al., 2010). The seasonal variation in NPF occurrence frequency also differed among site categories.
In early autumn (September and October), NPF events occurred more frequent in regional background than in urban
background sites, likely due to the high emission of biogenic VOCs in rural areas in autumn (Salma et al., 2016). Furthermore,
the seasonal pattern of NPF events varied among mountain sites, as shown in Fig.3. This variability may be a result of the
290 upslope valley winds, which can have different impact on different sites and seasons depending on the altitude and topography
of the site (Nieminen et al., 2018).

3.2 Growth and formation rates

Figure 4 shows the basic statistics of annual GR_{10-25} , J_{10-25} and CS at the nine GUAN sites. The growth and formation rate were
only evaluated for class I event in this study, and the CS was estimated for all NPF event days. As listed in Table 2, the annual
295 mean GR_{10-25} for particle sizes of 10–25 nm varied from 3.7 to 4.7 $nm\ h^{-1}$, with surprisingly minor differences between the
sites. Previous studies also found that GR varies little among different sites and exhibits only very weak dependency on the
low-volatility vapor concentration, particularly in a fixed site (Kulmala et al., 2022a, 2023). However, the site-to-site
comparison of J_{10-25} implied that stronger anthropogenic influences could lead to a higher J_{10-25} , which was consistent with
previous studies (e.g. Bousiotis et al., 2021b; Nieminen et al., 2018; Sebastian et al., 2022). The CS values were generally
300 higher in the area with stronger anthropogenic emissions, and the lowest at high Alpine site ZSF. The CS and J_{10-25} at BOS
were lower than the other two UB sites in Leipzig, suggesting relatively fewer anthropogenic emissions at BOS than LTR and
LWE. Additionally, one should be noticed that both LTR and LWE are located in the urban background of Leipzig. The
occurrence frequency and starting time of NPF (Sect.3.3) were similar at the two sites, while the GR_{10-25} and J_{10-25} were not.
One possible explanation for such differences on GR_{10-25} and J_{10-25} may be the different surroundings of the two sites. LTR is
305 located on the top of a three-floor building about 100 m from a main road, therefore is relatively more influenced by traffic
emissions. The LWE is located in the park with 30 m distance from a minor road, so the impact of fresh traffic emission is
negligible (Birmili et al., 2016). In one of our previous studies, it was found that the particle number concentration at LTR was
higher than that at LWE, especially for traffic related size range N_{10-30} and N_{30-200} , with 10 % and 17 % higher, respectively
(Sun et al., 2009), indicating higher gaseous precursor concentration and thus stronger anthropogenic influence at LTR.

310 Figure 5 displays the annual GR measured at GUAN sites and other European sites (Boulon et al., 2011; Bousiotis et al.,
2019; Bousiotis et al., 2021b; Herrmann et al., 2015; Kalkavouras et al., 2020; Lee et al., 2020; Manninen et al., 2010;

Nieminen et al., 2014; Nieminen et al., 2018; Salma et al., 2016; Tröstl et al., 2015; Vaananen et al., 2013; Vana et al., 2016). For the GR values and the corresponding size range reported in those studies please refer to Table S2 in the supplementary material. The GR₁₀₋₂₅ for GUAN sites falls within the range of those reported in previous European studies. Caution should be taken that the differences in observation periods and size ranges of GR may influence the comparison among sites. In UB sites, the highest GR was reported at BUD, with the size range of 6–50 nm. LWE, KST and LTR showed the similar GR level, but the size range of GR at KST was 16.6–50 nm. The lowest GR in UB sites were observed at COP and HEL, with the evaluated size range of 5.8–30 and 3.4–30 nm, respectively. In RB sites, the GR at site CBW was about 6.6 nm h⁻¹, which was much higher than other RB sites. This high GR at CBW may be resulted from the short observation period in this study, from 1 Apr 2008 to 31 Mar 2009 (Manninen et al., 2010). Meanwhile, another study reported the seasonal variation of GR at CBW between 10 and 25 nm as well (Niemininen et al., 2018). The seasonal GR₁₀₋₂₅ ranged from 2.9 to 4.9 nm h⁻¹, which was similar with GR₁₀₋₂₅ at RB sites of GUAN. For LMT sites, the GR₁₀₋₂₅ at SCH and HPB were lower than the GR₇₋₂₀ at another two LMT sites PUY and OPM located in central France. Nieminen et al. (2018) also found that GR₁₀₋₂₅ at PUY was significantly higher than those at other LMT sites, possibly related to the vertical transport of particles within the boundary layer. For high altitude and remote sites, the GR₁₀₋₂₅ of ZSF was comparable to those of other sites.

Figures 6 and 7 present the seasonal GR₁₀₋₂₅ and J_{10-25} at GUAN sites in this study. Since GR₁₀₋₂₅ and J_{10-25} were only evaluated for class I events, there were NPF events observed in winter-time but no GR₁₀₋₂₅ and J_{10-25} evaluated at some sites, for example at NEU. The highest GR₁₀₋₂₅ was observed in summer for most sites, while the lowest in winter. Many previous studies have also reported such seasonal pattern, especially in regional background area, which have been attributed to enhanced biogenic aerosol precursors and stronger solar radiation during summer (Nieminen et al., 2014; Kerminen et al., 2018; Asmi et al., 2011). Both LTR and LWE are located in the city of Leipzig, and the different seasonal variation in GR₁₀₋₂₅ may be due to the different degree of urban emission at these two sites, as discussed in Sect.3.1. The seasonal variations of J_{10-25} were similar with the one of GR₁₀₋₂₅ in urban background and regional background sites, with the universal maximum in summer observed. However, a different seasonal pattern for the three mountain sites were observed, with the maximum in J_{10-25} being reached in spring. This seasonal behaviour was observed for the site HPB in another previous study by Nieminen et al. (2018) as well. Another exception to the seasonal pattern of GR₁₀₋₂₅ and J_{10-25} was NEU, which had clear lower GR₁₀₋₂₅ and J_{10-25} in summer than in spring, which may have been underestimated due to missing data.

3.3 Starting time of NPF events

Figure 8 shows the estimated starting time of class I events as a function of day of year. The starting time was initially estimated based on local time (UTC+1) and further converted to solar time according to the longitude of the sites. The PNSD observations in our dataset initiate from particle sizes from 5 or 10 nm at different sites (Table 1). However, starting time at 10 nm ($t_{10\text{ nm}}$) was not able to describe the actual occurrence time of nucleation. Therefore, $t_{10\text{ nm}}$ has been converted to the critical nucleation diameter of 2 nm ($t_{2\text{ nm}}$) using the GR₁₀₋₂₅ values by $t_{2\text{ nm}} = t_{10\text{ nm}} - \frac{(10-2)}{GR_{10-25}}$.

Typically, most NPF events started between 07:30 and 9:00 solar time at all GUAN sites. Seasonal variations in starting
345 time were evident, with earlier starting time in summer due to earlier sunrise. It is noteworthy that the differences in the starting
time of NPF events exist between sites, as shown in Fig.8 and Fig.S7 in the supplementary material. The three mountainous
sites (HPB, SCH, and ZSF) had the latest starting time around 09:00. Two UB sites LTR and LWE had the earliest starting
time around 07:30. Starting time at BOS and three RB sites (MEL, WAL, and NEU) is around 08:30. Since the use of solar
time has already eliminated the bias of local time relative to site longitude, the difference of starting time among sites mainly
350 stems from the different diurnal variation of precursor concentration and CS. Figure S8 shows the mean diurnal cycle of CS
on NPF days for all the nine GUAN sites. CS at UB sites increases rapidly during morning rush hour due to the strong traffic
emission in urban area, implying also an increase of precursor concentration. The ratio of sources and sinks may be changed
during this time period and further leads to earlier NPF starting time in urban area than RB sites. In the mountain area, the CS
starts to increase at about 08:00 and reaches its daily maximum in the late afternoon, meaning that it may take some time for
355 the development of the boundary layer and transport of the precursors upward after sunrise, resulting in late NPF starting time.

4 Results II: environmental and climate relevance effects

4.1 Contribution of NPF on ultrafine particles

NPF events are believed to be a significant source of UFP. In this section, the contribution of NPF on UFP number
concentration was qualitatively and quantitatively evaluated using two approaches by Salma et al. (2017) and Ma and Birmili
360 (2015).

4.1.1 Nucleation strength factor

Nucleation strength factor (NSF) is a simple metric to qualitatively estimate the relative concentration increment of UFP
number concentration on NPF days. As stated in Salma et al. (2017), an NSF of 1 indicates that the relative contribution of
NPF events to UFP is negligible, while a value >2 suggests that NPF can be considered as a dominant source of UFP at the
365 site on NPF days. Figure 9 compares the annual median NSF between the nine GUAN sites and those reported in an earlier
study by Bousiotis et al. (2021b). The NSF was around 2 for all regional background and mountainous sites, implying that
NPF events were the dominant source on NPF days in those environments. NSF was much lower in urban background sites,
typically ranging between 1 and 2. Ma and Birmili (2015) reported that aged traffic and other urban sources contributed around
40 % and 30 % to N_{5-100} and N_{20-100} at LTR, respectively. Higher anthropogenic emissions results in higher UFP number
concentration and thus lower NSF in urban area. In addition, such high contributions from anthropogenic sources lead to an
370 increased CS, causing more new particles to be scavenged by the more polluted atmosphere, resulting in lower NSF in urban
area.

4.1.2 Quantitative contribution to UFP

Another approach was further implemented to derive a quantitative average contribution of NPF to UFP. The diurnal cycle of UFP increment on NPF days with high and low solar radiation was estimated, as described in Ma and Birmili (2015). In our study, the UFPs were assumed to originate from “NPF” and “other sources”, in which “other sources” encompassed all non-NPF sources such as fresh local traffic, aged traffic, other urban sources, and regional backgrounds.

Figure 10 displays the absolute and relative contributions of NPF to UFP (N_{10-100}) at seven GUAN sites, and Fig.11 shows the monthly relative contributions. The analysis did not include BOS and ZSF due to the absence of solar radiation data. As seen in the two figures, the highest contribution of NPF to UFP was found for the regional background sites, with contributions of around 25 % at MEL and NEU, and 15 % at WAL. For the two urban background sites, LTR and LWE, the contributions of NPF were lower, accounting for 11 % and 15 % of N_{10-100} , respectively. As discussed in Ma and Birmili (2015), regional background aerosols contribute to UFP equally for urban background (LTR) and nearby regional background (MEL). However, some urban sources such as aged traffic also contribute to UFP in urban background, resulting in a lower relative contribution of NPF to UFP at urban background sites. Due to the low occurrence and low nucleation rate of NPF at the mountain sites (Table 2), the contribution of NPF to UFP was the lowest at HPB and SCH, accounting for 5 % and 9 % of N_{10-100} , respectively.

Pronounced seasonal variations of the relative contributions of NPF to UFP were found for all the seven GUAN sites (Fig.11), with higher contribution from May to August and almost no contribution in winter. The contribution of NPF to UFP is determined by many factors such as the frequency, nucleation rate and growth rate of NPF, as well as the concentration of particles from other sources. The contribution of NPF is proportional to the frequency of NPF if keep other factors unchanged. Therefore, the seasonal patterns of the relative contributions of NPF were very similar to the seasonal variation of NPF occurrence frequency for each site (Fig.3). The highest relative contributions of NPF to UFP were observed during summer (from May to August), with the range of 30 % ~ 48 % and 41 % ~ 56 % at urban background and regional background sites, respectively. However, the seasonal distributions of NPF contribution observed at the mountain sites were similar to the one of NPF occurrence frequency in Fig.3, peaking in spring from March to May with the value from 14 % to 23 %.

4.2 Contribution of NPF on cloud nuclei condensation (CCN)

To evaluate the potential contribution of NPF to CCN, the relative enhancement of CCN number concentration (N_{CCN} enhancement, denoted as $E_{N_{CCN}}$), which is the ratio between N_{CCN} after and prior to the NPF event, has been estimated following the approach proposed by previous studies (Kalkavouras et al., 2019; Ren et al., 2021). It should be noted that during a NPF event, both the newly formed particles and pre-existing particles can grow to CCN-relevant size. The pre-existing particles have larger diameters and may reach CCN-relevant size faster than newly formed particles, therefore may even have a larger contribution to CCN number concentration. Kalkavouras et al. (2019) stated that the pre-existing particles may induce a bias in the estimated CCN enhancement up to 50 %. It is difficult to decompose the contributions of the two parts. So that the $E_{N_{CCN}}$

405 estimated in this study was an integrated CCN number concentration enhancement contributed by both the two parts during NPF events.

Table 3 summarizes $E_{N_{CCN}}$ on NPF days in our study and other previous studies conducted in Europe. Our dataset shows a pattern similar to the results from previous studies (Rejano et al., 2021; Kerminen et al., 2012; Dameto et al., 2017; etc.), with higher $E_{N_{CCN}}$ for weaker influence of anthropogenic emissions. However, exceptions were found for sites BOS and NEU, where $E_{N_{CCN}}$ was much higher than the one at the other sites in the same site categories. The seasonal distribution of $E_{N_{CCN}}$ (Fig.S9 in the supplementary material) at BOS indicated that the elevated N_{CCN} enhancement may be due to a significantly higher $E_{N_{CCN}}$ in autumn. And the higher $E_{N_{CCN}}$ at NEU may be attributed to seasonal bias in data availability. The highest $E_{N_{CCN}}$ was observed in the three mountain sites, due to the low background PNC in those area (Kerminen et al., 2012).

When comparing our results with other studies in Table 3, it is important to proceed with caution that the significant variation in $E_{N_{CCN}}$ may result from different observation periods, assumed supersaturation, critical diameter D_C , and N_{CCN} estimation methods. However, some consistencies can still be found. For example, $E_{N_{CCN}}$ at the urban background site Vienna was similar to those at the urban background sites in GUAN, and $E_{N_{CCN}}$ values at regional background sites in Finland and Sweden are comparable to those for our sites. Other studies have reported $E_{N_{CCN}}$ for site MEL and HPB as well. The results from the present study are consistent with those from a long-term observation study by Ren et al. (2021), while lower than another short-term NPF case study by Wu et al. (2015).

420 The observed $E_{N_{CCN}}$ in this study revealed a clear relationship between $E_{N_{CCN}}$ and the degree of anthropogenic emission influence in diverse environments. However, it is important to bear in mind that the estimation of $E_{N_{CCN}}$ is based on a constant D_C and may result in overestimation, as stated by Wu et al. (2015). Besides, the $E_{N_{CCN}}$ estimation accounted only for NPF days, not for the entire observation period. That is, the NPF occurrence frequency was not taken into consideration. It needs to be careful when interpreting the $E_{N_{CCN}}$ values, especially for those high $E_{N_{CCN}}$ values in clean area in Table 3. Accounting for the high $E_{N_{CCN}}$ but low NPF occurrence frequency in those clean areas, it cannot conclude that NPFs have a significant impact on the overall CCN budget at those sites.

4.3 Impact of NPF on aerosol extinction coefficient

The growth of newly formed particles into large size during NPF may subsequently affect the bulk aerosol optical properties, and further impact the regional aerosol radiative forcing and climate. However, the impact of NPF on aerosol optical properties was discussed in only few studies. For instance, Shen et al. (2011) analysed the enhancement of aerosol extinction coefficient during the evolution of a NPF event in a regional background site in China. To investigate the contribution of NPF to aerosol extinction coefficient for diverse environments, the ratio of averaged aerosol extinction coefficient at 550 nm ($\sigma_{ext, 550 \text{ nm}}$) between after and before each NPF event, was evaluated in this section, namely $\sigma_{ext, 550 \text{ nm}}$ enhancement. The start and end point for each NPF event were adopted from those for N_{CCN} enhancement evaluation in Sect.4.2. The $\sigma_{ext, 550 \text{ nm}}$ enhancement and the corresponding statistically significance are listed in Table 4. Statistically insignificant contributions were found for the other sites, especially for polluted urban sites. However, NPF events occurring in areas with low background PNC and low

anthropogenic emissions, such as regional background site NEU and the three mountain sites, can significantly enhance $\sigma_{\text{ext}, 550 \text{ nm}}$ on NPF event days. These findings underscore the importance of considering the impact of NPF on optical properties when assessing aerosol radiative forcing, especially in remote regions. Besides, similar with the $E_{N_{\text{ccn}}}$ estimation, the enhancement of $\sigma_{\text{ext}, 550 \text{ nm}}$ was only for NPF days. The results in Table 4 cannot represent the NPF enhancement of $\sigma_{\text{ext}, 550 \text{ nm}}$ over the whole study periods.

When discussing the aforementioned environmental and climate relevance effects of NPF (Sect.4), it is important to bear in mind that the obtained contribution is likely to be underestimated. One reason is the potential of missing cases where NPF is relatively weak or interrupted by changed airmasses during measurements. These occurrences, known as “quiet NPFs”, have been found to contribute to the secondary particles in the atmosphere (Kulmala et al. 2022b). Another reason is that it is difficult to follow the growth of newly formed particles longer than a few hours (certainly less than a day) in a single-site measurement, yet the growing particles remain in the ultrafine range 1-3 days (the time it takes for them to reach CCN size). As a result of these considerations, a substantial portion of the ultrafine particles in the troposphere classified as “background” or “other sources” is actually formed by NPF, either via unclear or weak events or 1-3 days upwind from the measurement site, leading to an underestimation of the relevance effects discussed above.

5 Conclusion

Based on a five-year dataset of the German Ultrafine Aerosol Network (GUAN), this study investigated the characteristics of NPF for various environments from urban background to high Alpine. The NPF occurrence frequencies show significant difference with respect to site categories, while the NPF occurrence frequencies at the sites in the same category were found to be similar. Regional background sites had the highest NPF occurrence frequency, with an average value of about 19 %, followed by urban background sites with an average of 15 %. NPF events were observed on 7 % of days at low mountain range sites and only 3 % of days at the high Alpine site ZSF. The NPF occurrence frequencies at GUAN sites in this work were found to be in the range of the occurrence frequency at other sites in Central Europe reported in previous studies.

The annual mean growth rate for particle sizes of 10–25 nm (GR_{10-25}) varied from 3.7 to 4.7 nm h⁻¹, with minor differences among sites. The annual formation rate J_{10-25} ranged from 0.4 to 2.9 cm⁻³ s⁻¹, increased with higher degree of anthropogenic emissions, implying the crucial role of anthropogenic precursors to NPF. The GR_{10-25} for GUAN site falls within the range of those reported in previous European studies. Obvious seasonal patterns of GR_{10-25} and J_{10-25} were observed, with the highest in summer, and the lowest in winter for urban and regional background sites. Different seasonal patterns for the three mountain sites were observed, with the maximum in J_{10-25} being reached in spring. Most NPF events started between 07:30 and 9:00 in solar time. Earlier starting time was found in summer due to earlier sunrise. The three mountainous sites had the latest starting time around 09:00. The two UB sites LTR and LWE had the earliest starting time around 07:30, while BOS and three RB sites around 08:30. The difference of starting time among sites mainly stems from the different diurnal variations of precursor concentration and CS.

The impact of NPF on ultrafine particles (UFPs), cloud condensation nuclei (CCN) and radiative forcing were quantitatively
470 evaluated and discussed. Over the entire observation periods, the contribution of NPF on UFP was about 13 %, 21 %, and 7 %
for the urban background, regional background, and low mountain range sites. The enhancement of CCN number concentration
on NPF days was found to be the highest and the most significant in mountain sites. Similarly, the enhancement of aerosol
extinction coefficient at 550 nm ($\sigma_{\text{ext},550 \text{ nm}}$) on NPF days was respectively 1.4, 1.8, 1.6, and 1.9 at site NEU, HPB, SCH, and
475 ZSF, while no statistically significant contributions were observed for the other sites. These findings underscore the importance
of considering the local environments of NPF when assessing its potential impact on regional climate in models. They also
emphasize the usefulness of a long-term aerosol measurement network with multiple sites for understanding the variation of
NPF features and their influencing factors over a regional scale.

Data availability

Datasets for this paper can be accessed at <https://ebas-data.nilu.no/Default.aspx> (Birmili et al., 2016).

480 Supplement

The supplement related to this article is available online at:

Author contributions

AW, NM, WB, MH, and JS designed the research. JS, YY, and NM conducted the data analysis with the help from VK and
MK. KaW, MM, TT, HF, BB, LR, CC, ME, RS, KW, FM, MS, OB, and BH conducted the measurements. JS and NM wrote
485 the paper with input from all co-authors.

Competing interests

At least one of the (co-)authors is a member of the editorial board of Atmospheric Chemistry and Physics. The peer-review
process was guided by an independent editor, and the authors also have no other competing interests to declare.

Disclaimer

490 Publisher's note: Copernicus Publications remains neutral with regard to jurisdictional claims in published maps and
institutional affiliations.

Acknowledgement

We acknowledge funding by the Chinese Postdoctoral Science Foundation (Certificate number:2023M740808), PI Project of Southern Marine Science and Engineering Guangdong Laboratory (Guangzhou) (GML2022005), and the German Federal Environment Ministry (BMU) grants F&E 370343200 (German title: Erfassung der Zahl feiner und ultrafeiner Partikel in der Außenluft) from 2008 to 2010, and F&E 371143232 (German title: Trendanalysen gesundheitsgefährdender Fein- und Ultrafeinstaubfraktionen unter Nutzung der im German Ultrafine Aerosol Network (GUAN) ermittelten Immissionsdaten durch Fortführung und Interpretation der Messreihen) from 2012 to 2013.

The authors would like to thank the technical and scientific staff members of the stations included in this study. André Sonntag and Stephan Nordmann (TROPOS/UBA) contributed to data processing. This work was also accomplished in the frame of the project ACTRIS-2 (Aerosols, Clouds, and Trace gases Research InfraStructure) under the European Union—Research Infrastructure Action in the frame of the H2020 program for “Integrating and opening existing national and regional research infrastructures of European interest” under Grant Agreement N654109 (Horizon 2020). Additionally, we acknowledge the WCCAP (World Calibration Centre for Aerosol Physics) as part of the WMO-GAW program base-funded by the UBA.

References

- Asmi, E., Kivekas, N., Kerminen, V.-M., Komppula, M., Hyvarinen, A.-P., Hatakka, J., Viisanen, Y., and Lihavainen, H.: Secondary new particle formation in Northern Finland Pallas site between the years 2000 and 2010, *Atmos. Chem. Phys.*, 11, 12959-12972, doi: 10.5194/acp-11-12959-2011, 2011.
- Baalbaki, R., Pikridas, M., Jokinen, T., Laurila, T., Dada, L., Bezantakos, S., Ahonen, L., Neitola, K., Maisser, A., Bimenyimana, E., Christodoulou, A., Unga, F., Savvides, C., Lehtipalo, K., Kangasluoma, J., Biskos, G., Petäjä, T., Kerminen, V. M., Sciare, J., and Kulmala, M.: Towards understanding the characteristics of new particle formation in the Eastern Mediterranean, *Atmos. Chem. Phys.*, 21, 9223-9251, doi: 10.5194/acp-21-9223-2021, 2021.
- Bianchi, F., Tröstl, J., Junninen, H., Frege, C., Henne, S., Hoyle, C.-R., Molteni, U., Herrmann, E., Adamov, A., Bukowiecki, N., Chen, X., Duplissy, J., Gysel, M., Hutterli, M., Kangasluoma, J., Kontkanen, J., Kürten, A., Manninen, H. E., Münch, S., Peräkylä, O., Petäjä, T., Rondo, L., Williamson, C., Weingartner, E., Curtius, J., Worsnop, D. R., Kulmala, M., Dommen, J., and Baltensperger, U.: New particle formation in the free troposphere: A question of chemistry and timing, *Science*, 352, 1109-1112, doi: 10.1126/science.aad5456, 2016.
- Birmili, W., Weinhold, K., Rasch, F., Sonntag, A., Sun, J., Merkel, M., Wiedensohler, A., Bastian, S., Schladitz, A., Löschau, G., Cyrys, J., Pitz, M., Gu, J., Kusch, T., Flentje, H., Quass, U., Kaminski, H., Kuhlbusch, T. A. J., Meinhardt, F., Schwerin, A., Bath, O., Ries, L., Gerwig, H., Wirtz, K., and Fiebig, M.: Long-term observations of tropospheric particle number size distributions and equivalent black carbon mass concentrations in the German Ultrafine Aerosol Network (GUAN), *Earth Syst. Sci. Data*, 8, 355-382, doi: 10.5194/essd-8-355-2016, 2016.

- 525 Birmili, W. and Wiedensohler, A.: New particle formation in the continental boundary layer: Meteorological and gas phase parameter influence, *Geophys. Res. Lett.*, 27, 3325-3328, doi: 10.1029/1999GL011221, 2000.
- Boulon, J., Sellegri, K., Hervo, M., Picard, D., Pichon, J.-M., Fréville, P., and Laj, P.: Investigation of nucleation events vertical extent: a long term study at two different altitude sites, *Atmos. Chem. Phys.*, 11, 5625-5639, doi: 10.5194/acp-11-5625-2011, 2011.
- 530 Bousiotis, D., Dall'Osto, M., Beddows, D.-C.-S., Pope, F.-D., and Harrison, R.-M.: Analysis of new particle formation (NPF) events at nearby rural, urban background and urban roadside sites, *Atmos. Chem. Phys.*, 19, 5679-5694, doi: 10.5194/acp-19-5679-2019, 2019.
- Bousiotis, D., Brean, J., Pope, F.-D., Dall'Osto, M., Querol, X., Alastuey, A., Perez, N., Petaja, T., Massling, A., Nojgaard, J. K., Nordstrom, C., Kouvarakis, G., Vratolis, S., Eleftheriadis, K., Niemi, J.-V., Portin, H., Wiedensohler, A., Weinhold, K., Merkel, M., Tuch, T., and Harrison, R.-M.: The effect of meteorological conditions and atmospheric composition in the occurrence and development of new particle formation (NPF) events in Europe, *Atmos. Chem. Phys.*, 21, 3345-3370, doi: 535 10.5194/acp-21-3345-2021, 2021a.
- Bousiotis, D., Pope, F.-D., Beddows, D.-C.-S., Dall'Osto, M., Massling, A., Nojgaard, J.-K., Nordstrom, C., Niemi, J.-V., Portin, H., Petaja, T., Perez, N., Alastuey, A., Querol, X., Kouvarakis, G., Mihalopoulos, N., Vratolis, S., Eleftheriadis, K., Wiedensohler, A., Weinhold, K., Merkel, M., Tuch, T., and Harrison, R.-M.: A phenomenology of new particle formation (NPF) at 13 European sites, *Atmos. Chem. Phys.*, 21, 11905-11925, doi: 10.5194/acp-21-11905-2021, 2021b.
- 540 Boy, M. and Kulmala, M.: Nucleation events in the continental boundary layer: Influence of physical and meteorological parameters, *Atmos. Chem. Phys.*, 2, 1-16, doi: 10.5194/acp-2-1-2002, 2002.
- Brines, M., Dall'Osto, M., Beddows, D.-C.-S., Harrison, R.-M., Gómez-Moreno, F., Núñez, L., Artñano, B., Costabile, F., Gobbi, G.-P., Salimi, F., Morawska, L., Sioutas, C., and Querol, X.: Traffic and nucleation events as main sources of ultrafine particles in high-insolation developed world cities, *Atmos. Chem. Phys.*, 15, 5929-5945, doi: 10.5194/acp-15-5929-2015, 2015.
- 545 Cai, R., Yang, D., Fu, Y., Wang, X., Li, X., Ma, Y., Hao, J., Zheng, J., and Jiang, J.: Aerosol surface area concentration: a governing factor in new particle formation in Beijing, *Atmos. Chem. Phys.*, 17, 12327-12340, doi: 10.5194/acp-17-12327-2017, 2017.
- 550 Casquero-Vera, J.-A., Lyamani, H., Dada, L., Hakala, S., Paasonen, P., Román, R., Fraile, R., Petäjä, T., Olmo-Reyes, F.-J., and Alados-Arboledas, L.: New particle formation at urban and high-altitude remote sites in the south-eastern Iberian Peninsula, *Atmos. Chem. Phys.*, 20, 14253-14271, doi: 10.5194/acp-20-14253-2020, 2020.
- Costabile, F., Birmili, W., Klose, S., Tuch, T., Wehner, B., Wiedensohler, A., Franck, U., König, K., and Sonntag, A.: Spatio-temporal variability and principal components of the particle number size distribution in an urban atmosphere, *Atmos. Chem. Phys.*, 9, 3163-3195, doi: 10.5194/acp-9-3163-2009, 2009.

- Dada, L., Paasonen, P., Nieminen, T., Buenrostro Mazon, S., Kontkanen, J., Peräkylä, O., Lehtipalo, K., Hussein, T., Petäjä, T., Kerminen, V.-M., Bäck, J., and Kulmala, M.: Long-term analysis of clear-sky new particle formation events and nonevents in Hyytiälä, *Atmos. Chem. Phys.*, 17, 6227-6241, doi: 10.5194/acp-17-6227-2017, 2017.
- 560 Dada, L., Ylivinkka, I., Baalbaki, R., Li, C., Guo, Y., Yan, C., Yao, L., Sarnela, N., Jokinen, T., Daellenbach, K.-R., Yin, R., Deng, C., Chu, B., Nieminen, T., Wang, Y., Lin, Z., Thakur, R. C., Kontkanen, J., Stolzenburg, D., Sipilä, M., Hussein, T., Paasonen, P., Bianchi, F., Salma, I., Weidinger, T., Pikridas, M., Sciare, J., Jiang, J., Liu, Y., Petäjä, T., Kerminen, V.-M., and Kulmala, M.: Sources and sinks driving sulfuric acid concentrations in contrasting environments: implications on proxy calculations, *Atmos. Chem. Phys.*, 20, 11747-11766, doi: 10.5194/acp-20-11747-2020, 2020.
- 565 Dal Maso, M., Kulmala, M., Riipinen, I., Wagner, R., Hussein, T., Aalto, P.-P., and Lehtinen, K.-E.: Formation and growth of fresh atmospheric aerosols: eight years of aerosol size distribution data from SMEAR II, Hyytiälä, Finland, *Boreal Environ. Res.*, 10, 323, 2005.
- Dall'Osto, M., Beddows, D.-C.-S., Asmi, A., Poulain, L., Hao, L., Freney, E., Allan, J.-D., Canagaratna, M., Crippa, M., Bianchi, F., de Leeuw, G., Eriksson, A., Swietlicki, E., Hansson, H.-C., Henzing, J.-S., Granier, C., Zemann, K., Laj, P., Onasch, T., Prevot, A., Putaud, J.-P., Sellegri, K., Vidal, M., Virtanen, A., Simo, R., Worsnop, D., O'Dowd, C., Kulmala, M., and Harrison, R.-M.: Novel insights on new particle formation derived from a pan-European observing system, *Scientific Reports*, 8, 1482, doi: 10.1038/s41598-017-17343-9, 2018.
- 570 Dameto de España, C., WonaSchütz, A., Steiner, G., Rosati, B., Demattio, A., Schuh, H., and Hitzenberger, R.: Long-term quantitative field study of New Particle Formation (NPF) events as a source of Cloud Condensation Nuclei (CCN) in the urban background of Vienna, *Atmos. Environ.*, 164, 289-298, doi: 10.1016/j.atmosenv.2017.06.001, 2017.
- 575 Ehn, M., Thornton, J.-A., Kleist, E., Sipilä, M., Junninen, H., Pullinen, I., Springer, M., Rubach, F., Tillmann, R., Lee, B., Lopez-Hilfiker, F., Andres, S., Acir, I.-H., Rissanen, M., Jokinen, T., Schobesberger, S., Kangasluoma, J., Kontkanen, J., Nieminen, T., Kurten, T., Nielsen, L.-B., Jorgensen, S., Kjaergaard, H.-G., Canagaratna, M., Dal Maso, M., Berndt, T., Petaja, T., Wahner, A., Kerminen, V.-M., Kulmala, M., Worsnop, D.-R., Wildt, J., and Mentel, T.-F.: A large source of low-volatility secondary organic aerosol, *Nature*, 506, 476-479, doi: 10.1038/nature13032, 2014.
- 580 Flentje, H., Claude, H., Elste, T., Gilge, S., Köhler, U., Plass-Dülmer, C., Steinbrecht, W., Thomas, W., Werner, A., and Fricke, W.: The Eyjafjallajökull eruption in April 2010 – detection of volcanic plume using in-situ measurements, ozone sondes and lidar-ceilometer profiles, *Atmos. Chem. Phys.*, 10, 10085-10092, doi: 10.5194/acp-10-10085-2010, 2010
- Größ, J., Hamed, A., Sonntag, A., Spindler, G., Manninen, H.-E., Nieminen, T., Kulmala, M., Hörrak, U., Plass-Dülmer, C., Wiedensohler, A., and Birmili, W.: Atmospheric new particle formation at the research station Melpitz, Germany: connection with gaseous precursors and meteorological parameters, *Atmos. Chem. Phys.*, 18, 1835-1861, doi: 10.5194/acp-18-1835-2018, 2018.
- 585 Hanson, D.-R., Bier, I., Panta, B., Jen, C.-N., and McMurry, P.-H.: Computational Fluid Dynamics Studies of a Flow Reactor: Free Energies of Clusters of Sulfuric Acid with NH₃ or Dimethyl Amine, *The Journal of Physical Chemistry A*, 121, 3976-3990, doi: 10.1021/acs.jpca.7b00252, 2017.

- 590 Herrmann, E., Weingartner, E., Henne, S., Vuilleumier, L., Bukowiecki, N., Steinbacher, M., Conen, F., Collaud Coen, M.,
Hammer, E., Jurányi, Z., Baltensperger, U., and Gysel, M.: Analysis of long-term aerosol size distribution data from
Jungfraujoch with emphasis on free tropospheric conditions, cloud influence, and air mass transport, *Geophys. Res.*, 120,
9459-9480, doi: 10.1002/2015JD023660, 2015.
- Hirshorn, N.-S., Zuromski, L.-M., Rapp, C., McCubbin, I., Carrillo-Cardenas, G., Yu, F., and Hallar, A.-G.: Seasonal
595 significance of new particle formation impacts on cloud condensation nuclei at a mountaintop location, *Atmos. Chem. Phys.*,
22, 15909-15924, doi: 10.5194/acp-22-15909-2022, 2022.
- Hofman, J., Staelens, J., Cordell, R., Stroobants, C., Zikova, N., Hama, S.-M.-L., Wyche, K.-P., Kos, G.-P.-A., Van der Zee,
S., Smallbone, K.-L., Weijers, E.-P., Monks, P.-S., and Roekens, E.: Ultrafine particles in four European urban
environments: Results from a new continuous long-term monitoring network, *Atmos. Environ.*, 136, 68-81, doi:
600 10.1016/j.atmosenv.2016.04.010, 2016.
- Joutsensaari, J., Ozon, M., Nieminen, T., Mikkonen, S., Lahivaara, T., Decesari, S., Facchini, M.-C., Laaksonen, A., and
Lehtinen, K.-E.-J.: Identification of new particle formation events with deep learning, *Atmos. Chem. Phys.*, 18, 9597-9615,
doi: 10.5194/acp-18-9597-2018, 2018.
- Kalkavouras, P., Bougiatioti, A., Kalivitis, N., Stavroulas, I., Tombrou, M., Nenes, A., and Mihalopoulos, N.: Regional new
605 particle formation as modulators of cloud condensation nuclei and cloud droplet number in the eastern Mediterranean,
Atmos. Chem. Phys., 19, 6185-6203, doi: 10.5194/acp-19-6185-2019, 2019.
- Kalkavouras, P., Bougiatioti, A., Grivas, G., Stavroulas, I., Kalivitis, N., Liakakou, E., Gerasopoulos, E., Pilinis, C., and
Mihalopoulos, N.: On the regional aspects of new particle formation in the Eastern Mediterranean: A comparative study
between a background and an urban site based on long term observations, *Atmos. Res.*, 239, doi:
610 10.1016/j.atmosres.2020.104911, 2020.
- Kecorius, S., Vogl, T., Paasonen, P., Lampilahti, J., Rothenberg, D., Wex, H., Zeppenfeld, S., van Pinxteren, M., Hartmann,
M., Henning, S., Gong, X., Welti, A., Kulmala, M., Stratmann, F., Herrmann, H., and Wiedensohler, A.: New particle
formation and its effect on cloud condensation nuclei abundance in the summer Arctic: a case study in the Fram Strait and
Barents Sea, *Atmos. Chem. Phys.*, 19, 14339-14364, doi: 10.5194/acp-19-14339-2019, 2019.
- 615 Kerminen, V.-M., Pirjola, L., and Kulmala, M.: How significantly does coagulation limit atmospheric particle
production?, *J. Geophys. Res.-Atmos.*, 106, 24119-24125, doi: 10.1029/2001jd000322, 2001.
- Kerminen, V.-M., Chen, X.-M., Vakkari, V., Petaja, T., Kulmala, M., and Bianchi, F.: Atmospheric new particle formation
and growth: review of field observations, *Environmental Research Letters*, 13, doi:10.1088/1748-9326/aadf3c, 2018.
- Kerminen, V.-M., Paramonov, M., Anttila, T., Riipinen, I., Fountoukis, C., Korhonen, H., Asmi, E., Laakso, L., Lihavainen,
620 H., Swietlicki, E., Svenningsson, B., Asmi, A., Pandis, S.-N., Kulmala, M., and Petäjä, T.: Cloud condensation nuclei
production associated with atmospheric nucleation: a synthesis based on existing literature and new results, *Atmos. Chem.
Phys.*, 12, 12037-12059, doi: 10.5194/acp-12-12037-2012, 2012.

- 625 Kulmala, M., Petäjä, T., Nieminen, T., Sipilä, M., Manninen, H.-E., Lehtipalo, K., Dal Maso, M., Aalto, P.-P., Junninen, H., Paasonen, P., Riipinen, I., Lehtinen, K.-E.-J., Laaksonen, A., and Kerminen, V.-M.: Measurement of the nucleation of atmospheric aerosol particles, *Nature Protocols*, 7, 1651-1667, doi: 10.1038/nprot.2012.091, 2012.
- Kulmala, M., Petaja, T., Ehn, M., Thornton, J., Sipila, M., Worsnop, D.-R., and Kerminen, V.-M.: Chemistry of Atmospheric Nucleation: On the Recent Advances on Precursor Characterization and Atmospheric Cluster Composition in Connection with Atmospheric New Particle Formation, *Annu. Rev. Phys. Chem.*, 65, 21-37, doi: 10.1146/annurev-physchem-040412-110014, 2014.
- 630 Kulmala, M., Cai, R., Stolzenburg, D., Zhou, Y., Dada, L., Guo, Y., Yan, C., Petäjä, T., Jiang, J., and Kerminen, V.-M.: The contribution of new particle formation and subsequent growth to haze formation, *Environmental Science: Atmospheres*, 2, 352-361, doi: 10.1039/D1EA00096A, 2022a.
- Kulmala, M., Junninen, H., Dada, L., Salma, I., Weidinger, T., Thén, W., Vörösmarty, M., Komsaare, K., Stolzenburg, D., Cai, R., Yan, C., Li, X., Deng, C., Jiang, J., Petäjä, T., Nieminen, T., and Kerminen, V.-M.: Quiet New Particle Formation
635 in the Atmosphere, *Frontiers in Environmental Science*, 10, doi: 10.3389/fenvs.2022.912385, 2022b.
- Kulmala, M., Cai, R.-L., Ezhova, E., Deng, C.-J., Stolzenburg, D., Dada, L., Guo, Y.-S., Yan, C., Perakyla, O., Lintunen, A., Nieminen, T., Kokkonen, T.-V., Sarnela, N., Petaja, T., and Kerminen, V.-M.: Direct link between the characteristics of atmospheric new particle formation and Continental Biosphere-Atmosphere-Cloud-Climate (COBACC) feedback loop, *Boreal Environ. Res.*, 28, 1-13, 2023.
- 640 Kürten, A., Bergen, A., Heinritzi, M., Leiminger, M., Lorenz, V., Piel, F., Simon, M., Sitals, R., Wagner, A.-C., and Curtius, J.: Observation of new particle formation and measurement of sulfuric acid, ammonia, amines and highly oxidized organic molecules at a rural site in central Germany, *Atmos. Chem. Phys.*, 16, 12793-12813, doi: 10.5194/acp-16-12793-2016, 2016.
- Kürten, A., Li, C., Bianchi, F., Curtius, J., Dias, A., Donahue, N.-M., Duplissy, J., Flagan, R.-C., Hakala, J., Jokinen, T.,
645 Kirkby, J., Kulmala, M., Laaksonen, A., Lehtipalo, K., Makhmutov, V., Onnela, A., Rissanen, M.-P., Simon, M., Sipilä, M., Stozhkov, Y., Tröstl, J., Ye, P., and McMurry, P.-H.: New particle formation in the sulfuric acid–dimethylamine–water system: reevaluation of CLOUD chamber measurements and comparison to an aerosol nucleation and growth model, *Atmos. Chem. Phys.*, 18, 845-863, doi: 10.5194/acp-18-845-2018, 2018.
- Laaksonen, A., Kulmala, M., O'Dowd, C.-D., Joutsensaari, J., Vaattovaara, P., Mikkonen, S., Lehtinen, K.-E.-J., Sogacheva,
650 L., Dal Maso, M., Aalto, P., Petäjä, T., Sogachev, A., Yoon, Y.-J., Lihavainen, H., Nilsson, D., Facchini, M.-C., Cavalli, F., Fuzzi, S., Hoffmann, T., Arnold, F., Hanke, M., Sellegri, K., Umann, B., Junkermann, W., Coe, H., Allan, J.-D., Alfarra, M.-R., Worsnop, D.-R., Riekkola, M.-L., Hyötyläinen, T., and Viisanen, Y.: The role of VOC oxidation products in continental new particle formation, *Atmos. Chem. Phys.*, 8, 2657-2665, doi: 10.5194/acp-8-2657-2008, 2008.
- Lee, H., Lee, K., Lunder, C.-R., Krejci, R., Aas, W., Park, J., Park, K.-T., Lee, B.-Y., Yoon, Y.-J., and Park, K.: Atmospheric
655 new particle formation characteristics in the Arctic as measured at Mount Zeppelin, Svalbard, from 2016 to 2018, *Atmos. Chem. Phys.*, 20, 13425-13441, doi: 10.5194/acp-20-13425-2020, 2020.

- Lee, S.-H., Gordon, H., Yu, H., Lehtipalo, K., Haley, R., Li, Y., and Zhang, R.: New Particle Formation in the Atmosphere: From Molecular Clusters to Global Climate, *Geophys. Res.*, 124, 7098-7146, doi:10.1029/2018JD029356, 2019.
- Li, X., Chee, S., Hao, J., Abbatt, J.-P.-D., Jiang, J., and Smith, J.-N.: Relative humidity effect on the formation of highly oxidized molecules and new particles during monoterpene oxidation, *Atmos. Chem. Phys.*, 19, 1555-1570, doi: 10.5194/acp-19-1555-2019, 2019.
- Ma, N. and Birmili, W.: Estimating the contribution of photochemical particle formation to ultrafine particle number averages in an urban atmosphere, *Science of The Total Environment*, 512–513, 154-166, doi: 10.1016/j.scitotenv.2015.01.009, 2015.
- Mäkelä, J.-M., Aalto, P., Jokinen, V., Pohja, T., Nissinen, A., Palmroth, S., Markkanen, T., Seitsonen, K., Lihavainen, H., and Kulmala, M.: Observations of ultrafine aerosol particle formation and growth in boreal forest. *Geophys. Res. Lett.*, 24(10), 1219-1222, doi: 10.1029/97GL00920, 1997.
- Manninen, H.-E., Nieminen, T., Asmi, E., Gagné, S., Häkkinen, S., Lehtipalo, K., Aalto, P., Vana, M., Mirme, A., Mirme, S., Hörrak, U., Plass-Dülmer, C., Stange, G., Kiss, G., Hoffer, A., Törő, N., Moerman, M., Henzing, B., de Leeuw, G., Brinkenberg, M., Kouvarakis, G.-N., Bougiatioti, A., Mihalopoulos, N., O'Dowd, C., Ceburnis, D., Arneth, A., Svenningsson, B., Swietlicki, E., Tarozzi, L., Decesari, S., Facchini, M.-C., Birmili, W., Sonntag, A., Wiedensohler, A., Boulon, J., Sellegri, K., Laj, P., Gysel, M., Bukowiecki, N., Weingartner, E., Wehrle, G., Laaksonen, A., Hamed, A., Joutsensaari, J., Petäjä, T., Kerminen, V.-M., and Kulmala, M.: EUCAARI ion spectrometer measurements at 12 European sites – analysis of new particle formation events, *Atmos. Chem. Phys.*, 10, 7907-7927, doi: 10.5194/acp-10-7907-2010, 2010.
- Mie, G.: Articles on the optical characteristics of turbid tubes, especially colloidal metal solutions, *Annalen Der Physik*, 25, 377-445, doi: 10.1002/andp.19083300302, 1908.
- Németh, Z. and Salma, I.: Spatial extension of nucleating air masses in the Carpathian Basin, *Atmos. Chem. Phys.*, 14, 8841-8848, doi: 10.5194/acp-14-8841-2014, 2014.
- Németh, Z., Rosati, B., Zíková, N., Salma, I., Bozó, L., Dameto de España, C., Schwarz, J., Ždímal, V., and Wonaschütz, A.: Comparison of atmospheric new particle formation events in three Central European cities, *Atmos. Environ.*, 178, 191-197, doi: 10.1016/j.atmosenv.2018.01.035, 2018.
- Nieminen, T., Asmi, A., Dal Maso, M., Aalto, P., Keronen, P., Petaja, T., Kulmala, M., and Kerminen, V.-M.: Trends in atmospheric new-particle formation: 16 years of observations in a boreal-forest environment, *Boreal Environ. Res.*, 19, 191-214, 2014.
- Nieminen, T., Kerminen, V.-M., Petaja, T., Aalto, P.-P., Arshinov, M., Asmi, E., Baltensperger, U., Beddows, D.-C.-S., Beukes, J.-P., Collins, D., Ding, A.-J., Harrison, R.-M., Henzing, B., Hooda, R., Hu, M., Horrak, U., Kivekas, N., Komsaare, K., Krejci, R., Kristensson, A., Laakso, L., Laaksonen, A., Leitch, W.-R., Lihavainen, H., Mihalopoulos, N., Nemeth, Z., Nie, W., O'Dowd, C., Salma, I., Sellegri, K., Svenningsson, B., Swietlicki, E., Tunved, P., Ulevicius, V., Vakkari, V., Vana, M., Wiedensohler, A., Wu, Z.-J., Virtanen, A., and Kulmala, M.: Global analysis of continental boundary layer new particle

- 690 formation based on long-term measurements, *Atmos. Chem. Phys.*, 18, 14737-14756, doi: 10.5194/acp-18-14737-2018, 2018.
- O'Dowd, C.-D., Geever, M., and Hill, M.-K.: New particle formation: Nucleation rates and spatial scales in the clean marine coastal environment, *Geophys. Res. Lett.*, 25, 1661-1664, doi: 10.1029/98gl01005, 1998.
- Petäjä, T., Mauldin, I.-R.-L., Kosciuch, E., McGrath, J., Nieminen, T., Paasonen, P., Boy, M., Adamov, A., Kotiaho, T., and
695 Kulmala, M.: Sulfuric acid and OH concentrations in a boreal forest site, *Atmos. Chem. Phys.*, 9, 7435-7448, doi: 10.5194/acp-9-7435-2009, 2009.
- Pfeifer, S., Birmili, W., Schladitz, A., Müller, T., Nowak, A., and Wiedensohler, A.: A fast and easy-to-implement inversion algorithm for mobility particle size spectrometers considering particle number size distribution information outside of the detection range, *Atmos. Meas. Tech.*, 7, 95-105, doi: 10.5194/amt-7-95-2014, 2014.
- 700 Plauskaite, K., Ulevicius, V., Spirkauskaitė, N., Bycenkiene, S., Zielinski, T., Petelski, T., and Ponczkowska, A.: Observations of new particle formation events in the south-eastern Baltic Sea, *Oceanologia*, 52, 53-75, doi: 10.5697/oc.52-1.053, 2010.
- Qi, X.-M., Ding, A.-J., Roldin, P., Xu, Z.-N., Zhou, P.-T., Sarnela, N., Nie, W., Huang, X., Rusanen, A., Ehn, M., Rissanen, M.-P., Petaja, T., Kulmala, M., and Boy, M.: Modelling studies of HOMs and their contributions to new particle formation and growth: comparison of boreal forest in Finland and a polluted environment in China, *Atmos. Chem. Phys.*, 18, 11779-
705 11791, doi: 10.5194/acp-18-11779-2018, 2018.
- Rejano, F., Titos, G., Casquero-Vera, J.-A., Lyamani, H., Andrews, E., Sheridan, P., Cazorla, A., Castillo, S., Alados-Arboledas, L., and Olmo, F.-J.: Activation properties of aerosol particles as cloud condensation nuclei at urban and high-altitude remote sites in southern Europe, *Science of The Total Environment*, 762, 143100, doi: 10.1016/j.scitotenv.2020.143100, 2021.
- 710 Ren, J.-Y., Chen, L., Fan, T.-Y., Liu, J.-Y., Jiang, S.-H., and Zhang, F.: The NPF Effect on CCN Number Concentrations: A Review and Re-Evaluation of Observations From 35 Sites Worldwide, *Geophys. Res. Lett.*, 48, doi: 10.1029/2021gl095190, 2021.
- Rose, C., Sellegri, K., Moreno, I., Velarde, F., Ramonet, M., Weinhold, K., Krejci, R., Andrade, M., Wiedensohler, A., Ginot, P., and Laj, P.: CCN production by new particle formation in the free troposphere, *Atmos. Chem. Phys.*, 17, 1529-1541,
715 doi: 10.5194/acp-17-1529-2017, 2017.
- Salma, I., Németh, Z., Kerminen, V.-M., Aalto, P., Nieminen, T., Weidinger, T., Molnár, Á., Imre, K., and Kulmala, M.: Regional effect on urban atmospheric nucleation, *Atmos. Chem. Phys.*, 16, 8715-8728, doi: 10.5194/acp-16-8715-2016, 2016.
- Salma, I. and Németh, Z.: Dynamic and timing properties of new aerosol particle formation and consecutive growth events,
720 *Atmos. Chem. Phys.*, 19, 5835-5852, doi: 10.5194/acp-19-5835-2019, 2019.
- Salma, I., Varga, V., and Németh, Z.: Quantification of an atmospheric nucleation and growth process as a single source of aerosol particles in a city, *Atmos. Chem. Phys.*, 17, 15007-15017, doi: 10.5194/acp-17-15007-2017, 2017.

- Salvador, P., Barreiro, M., Gomez-Moreno, F.-J., Alonso-Blanco, E., and Artinano, B.: Synoptic classification of meteorological patterns and their impact on air pollution episodes and new particle formation processes in a south European air basin, *Atmos. Environ.*, 245, doi: 10.1016/j.atmosenv.2020.118016, 2021.
- 725 Sebastian, M., Kompalli, S.-K., Kumar, V.-A., Jose, S., Babu, S.-S., Pandithurai, G., Singh, S., Hooda, R.-K., Soni, V.-K., Pierce, J.-R., Vakkari, V., Asmi, E., Westervelt, D.-M., Hyvarinen, A.-P., and Kanawade, V.-P.: Observations of particle number size distributions and new particle formation in six Indian locations, *Atmos. Chem. Phys.*, 22, 4491-4508, doi: 10.5194/acp-22-4491-2022, 2022.
- 730 Seinfeld, J.-H., Pandis, S.-N., and Noone, K.: *Atmospheric Chemistry and Physics: From Air Pollution to Climate Change*, *Physics Today*, 51, 88-90, doi: 10.1063/1.882420, 1998.
- Sellegri, K., Rose, C., Marinoni, A., Lupi, A., Wiedensohler, A., Andrade, M., Bonasoni, P., and Laj, P.: New Particle Formation: A Review of Ground-Based Observations at Mountain Research Stations, *Atmosphere*, 10, 493, doi: 10.3390/atmos10090493, 2019.
- 735 Shen, X., Sun, J., Zhang, X., Kivekäs, N., Zhang, Y., Wang, T., Zhang, X., Yang, Y., Wang, D., Zhao, Y., and Qin, D.: Particle Climatology in Central East China Retrieved from Measurements in Planetary Boundary Layer and in Free Troposphere at a 1500-m-High Mountaintop Site, *Aerosol Air Qual. Res.*, 16, 689-701, doi: 10.4209/aaqr.2015.02.0070, 2016.
- Shen, X.-J., Sun, J.-Y., Zhang, Y.-M., Wehner, B., Nowak, A., Tuch, T., Zhang, X.-C., Wang, T.-T., Zhou, H.-G., Zhang, X.-
740 L., Dong, F., Birmili, W., and Wiedensohler, A.: First long-term study of particle number size distributions and new particle formation events of regional aerosol in the North China Plain, *Atmos. Chem. Phys.*, 11, 1565-1580, doi: 10.5194/acp-11-1565-2011, 2011.
- Sihto, S.-L., Mikkilä, J., Vanhanen, J., Ehn, M., Liao, L., Lehtipalo, K., Aalto, P.-P., Duplissy, J., Petäjä, T., Kerminen, V.-
745 M., Boy, M., and Kulmala, M.: Seasonal variation of CCN concentrations and aerosol activation properties in boreal forest, *Atmos. Chem. Phys.*, 11, 13269-13285, doi: 10.5194/acp-11-13269-2011, 2011.
- Smejkalova, A.-H., Zikova, N., Zdimal, V., Placha, H., and Bitter, M.: Atmospheric aerosol growth rates at different background station types, *Environ. Sci. Pollut. Res.*, 28, 13352-13364, doi: 10.1007/s11356-020-11424-5, 2021.
- Spindler, G., Grüner, A., Müller, K., Schlimper, S., and Herrmann, H.: Long-term size-segregated particle (PM₁₀, PM_{2.5}, PM₁) characterization study at Melpitz influence of air mass inflow, weather conditions and season, *J Atmos Chem*, 70,
750 165-195, doi: 10.1007/s10874-013-9263-8, 2013.
- Sun, J., Birmili, W., Hermann, M., Tuch, T., Weinhold, K., Spindler, G., Schladitz, A., Bastian, S., Löschau, G., Cyrys, J., Gu, J., Flentje, H., Briel, B., Asbach, C., Kaminski, H., Ries, L., Sohmer, R., Gerwig, H., Wirtz, K., Meinhardt, F., Schwerin, A., Bath, O., Ma, N., and Wiedensohler, A.: Variability of black carbon mass concentrations, sub-micrometer particle number concentrations and size distributions: results of the German Ultrafine Aerosol Network ranging from city street to
755 High Alpine locations, *Atmos. Environ.*, 202, 256-268, doi: 10.1016/j.atmosenv.2018.12.029, 2019.

- Sun, J., Birmili, W., Hermann, M., Tuch, T., Weinhold, K., Merkel, M., Rasch, F., Müller, T., Schladitz, A., Bastian, S., Löschau, G., Cyrys, J., Gu, J., Flentje, H., Briel, B., Asbach, C., Kaminski, H., Ries, L., Sohmer, R., Gerwig, H., Wirtz, K., Meinhardt, F., Schwerin, A., Bath, O., Ma, N., and Wiedensohler, A.: Decreasing trends of particle number and black carbon mass concentrations at 16 observational sites in Germany from 2009 to 2018, *Atmos. Chem. Phys.*, 20, 7049-7068, doi: 10.5194/acp-20-7049-2020, 2020.
- 760 Sun, J., Hermann, M., Yuan, Y., Birmili, W., Collaud Coen, M., Weinhold, K., Madueño, L., Poulain, L., Tuch, T., Ries, L., Sohmer, R., Couret, C., Frank, G., Brem, B. T., Gysel-Beer, M., Ma, N., and Wiedensohler, A.: Long-term trends of black carbon and particle number concentration in the lower free troposphere in Central Europe, *Environmental Sciences Europe*, 33, doi: 10.1186/s12302-021-00488-w, 2021.
- 765 Swietlicki, E., Hansson, H.-C., Hämeri, K., Svenningsson, B., Massling, A., McFiggans, G., McMurry, P., Petäjä, T., Tunved, P., and Gysel, M.: Hygroscopic properties of submicrometer atmospheric aerosol particles measured with H-TDMA instruments in various environments—a review, *Tellus B: Chemical and Physical Meteorology*, 60, 432-469, doi: 10.1111/j.1600-0889.2008.00350.x, 2008.
- 770 Tröstl, J., Herrmann, E., Frege, C., Bianchi, F., Molteni, U., Bukowiecki, N., Hoyle, C.-R., Steinbacher, M., Weingartner, E., Dommen, J., Gysel, M., and Baltensperger, U.: Contribution of new particle formation to the total aerosol concentration at the high-altitude site Jungfrauoch (3580 m a.s.l., Switzerland), *Geophys. Res.* , 121, 11,692-611,711, doi: 10.1002/2015JD024637, 2016.
- Vaananen, R., Kyro, E.-M., Nieminen, T., Kivekas, N., Junninen, H., Virkkula, A., Dal Maso, M., Lihavainen, H., Viisanen, Y., Svenningsson, B., Holst, T., Arneth, A., Aalto, P.-P., Kulmala, M., and Kerminen, V.-M.: Analysis of particle size distribution changes between three measurement sites in northern Scandinavia, *Atmos. Chem. Phys.*, 13, 11887-11903, doi: 10.5194/acp-13-11887-2013, 2013.
- 775 Vana, M., Komsaare, K., Horrak, U., Mirme, S., Nieminen, T., Kontkanen, J., Manninen, H.-E., Petaja, T., Noe, S.-M., and Kulmala, M.: Characteristics of new-particle formation at three SMEAR stations, *Boreal Environ. Res.*, 21, 345-362, 2016.
- 780 Wang, D., Guo, H., Cheung, K., and Gan, F.: Observation of nucleation mode particle burst and new particle formation events at an urban site in Hong Kong, *Atmos. Environ.*, 99, 196-205, doi: 10.1016/j.atmosenv.2014.09.074, 2014.
- Wang, Z., Birmili, W., Hamed, A., Wehner, B., Spindler, G., Pei, X., Wu, Z., Cheng, Y., Su, H., and Wiedensohler, A.: Contributions of volatile and nonvolatile compounds (at 300°C) to condensational growth of atmospheric nanoparticles: An assessment based on 8.5 years of observations at the Central Europe background site Melpitz, *J. Geophys. Res.-Atmos.*, 122, 485-497, doi: 10.1002/2016JD025581, 2017.
- 785 Wex, H., Neususs, C., Wendisch, M., Stratmann, F., Koziar, C., Keil, A., Wiedensohler, A., and Ebert, M.: Particle scattering, backscattering, and absorption coefficients: An in-situ closure and sensitivity study, *J. Geophys. Res.-Atmos.*, 107, doi: 10.1029/2000jd000234, 2002.
- Wiedensohler, A.: An approximation of the bipolar charge distribution for particles in the submicron range, *J. Aerosol Sci.*, 19, 387-389, 1988.

- 790 Wiedensohler, A., Birmili, W., Nowak, A., Sonntag, A., Weinhold, K., Merkel, M., Wehner, B., Tuch, T., Pfeifer, S., Fiebig,
M., Fjåraa, A.-M., Asmi, E., Sellegri, K., Depuy, R., Venzac, H., Villani, P., Laj, P., Aalto, P., Ogren, J.-A., Swietlicki, E.,
Williams, P., Roldin, P., Quincey, P., Hüglin, C., Fierz-Schmidhauser, R., Gysel, M., Weingartner, E., Riccobono, F.,
Santos, S., Gröning, C., Faloon, K., Beddows, D., Harrison, R., Monahan, C., Jennings, S.-G., O'Dowd, C.-D., Marinoni,
A., Horn, H.-G., Keck, L., Jiang, J., Scheckman, J., McMurry, P.-H., Deng, Z., Zhao, C.-S., Moerman, M., Henzing, B., de
795 Leeuw, G., Löschau, G., and Bastian, S.: Mobility particle size spectrometers: harmonization of technical standards and
data structure to facilitate high quality long-term observations of atmospheric particle number size distributions, *Atmos.
Meas. Tech.*, **5**, 657-685, doi: 10.5194/amt-5-657-2012, 2012.
- Wiedensohler, A., Wiesner, A., Weinhold, K., Birmili, W., Hermann, M., Merkel, M., Müller, T., Pfeifer, S., Schmidt, A.,
Tuch, T., Velarde, F., Quincey, P., Seeger, S., and Nowak, A.: Mobility particle size spectrometers: Calibration procedures
800 and measurement uncertainties, *Aerosol Sci. Technol.*, **52**, 146-164, doi: 10.1080/02786826.2017.1387229, 2018.
- Williamson, C.-J., Kupc, A., Axisa, D., Bilsback, K.-R., Bui, T., Campuzano-Jost, P., Dollner, M., Froyd, K.-D., Hodshire,
A.-L., Jimenez, J.-L., Kodros, J.-K., Luo, G., Murphy, D.-M., Nault, B.-A., Ray, E.-A., Weinzierl, B., Wilson, J.-C., Yu,
F.-Q., Yu, P.-F., Pierce, J.-R., and Brock, C.-A.: A large source of cloud condensation nuclei from new particle formation
in the tropics, *Nature*, **574**, 399-403, doi: 10.1038/s41586-019-1638-9, 2019.
- 805 Wu, Z.-J., Poulain, L., Birmili, W., Größ, J., Niedermeier, N., Wang, Z.-B., Herrmann, H., and Wiedensohler, A.: Some
insights into the condensing vapors driving new particle growth to CCN sizes on the basis of hygroscopicity measurements,
Atmos. Chem. Phys., **15**, 13071-13083, doi: 10.5194/acp-15-13071-2015, 2015.
- Yao, L., Garmash, O., Bianchi, F., Zheng, J., Yan, C., Kontkanen, J., Junninen, H., Mazon, S.-B., Ehn, M., Paasonen, P., Sipila,
M., Wang, M.-Y., Wang, X.-K., Xiao, S., Chen, H.-F., Lu, Y.-Q., Zhang, B.-W., Wang, D.-F., Fu, Q.-Y., Geng, F.-H., Li, L.,
810 Wang, H.-L., Qiao, L.-P., Yang, X., Chen, J.-M., Kerminen, V.-M., Petaja, T., Worsnop, D.-R., Kulmala, M., and Wang,
L.: Atmospheric new particle formation from sulfuric acid and amines in a Chinese megacity, *Science*, **361**, 278-281, doi:
10.1126/science.aao4839, 2018.
- Yuan, Y., Ries, L., Petermeier, H., Trickl, T., Leuchner, M., Couret, C., Sohmer, R., Meinhardt, F., and Menzel, A.: On the
diurnal, weekly, and seasonal cycles and annual trends in atmospheric CO₂ at Mount Zugspitze, Germany, during 1981–
815 2016, *Atmos. Chem. Phys.*, **19**, 999-1012, doi: 10.5194/acp-19-999-2019, 2019.

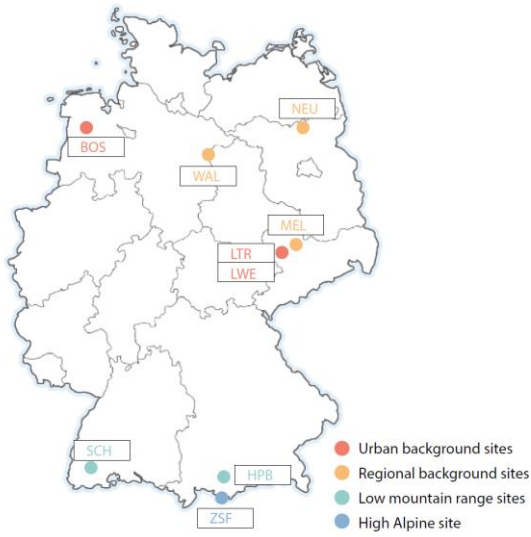
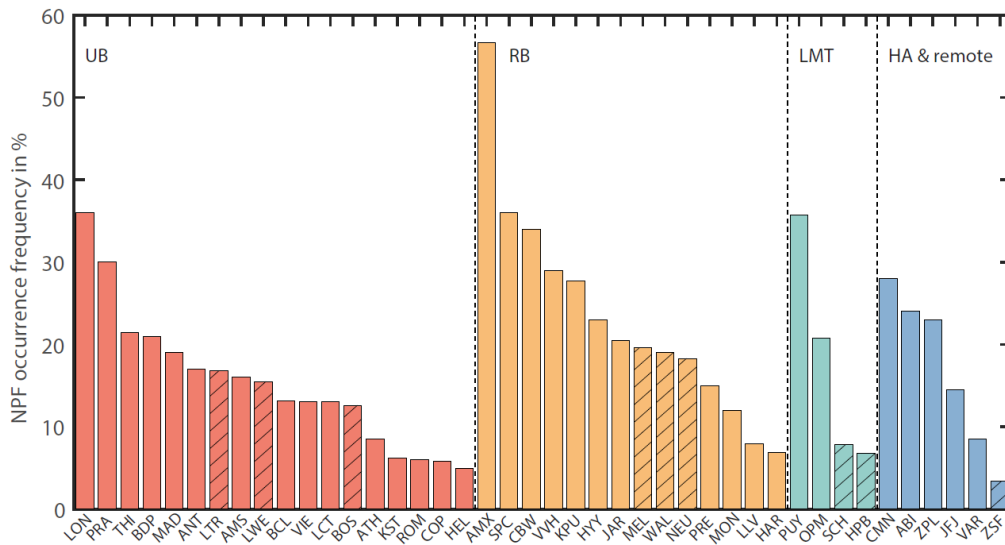


Figure 1: The locations of the nine selected observation sites in the German Ultrafine Aerosol Network (GUAN).



820 **Figure 2: Annual occurrence frequency of NPF events in the present study and other studies in Europe. The hatched pattern denotes the results for the GUAN sites in this study.**

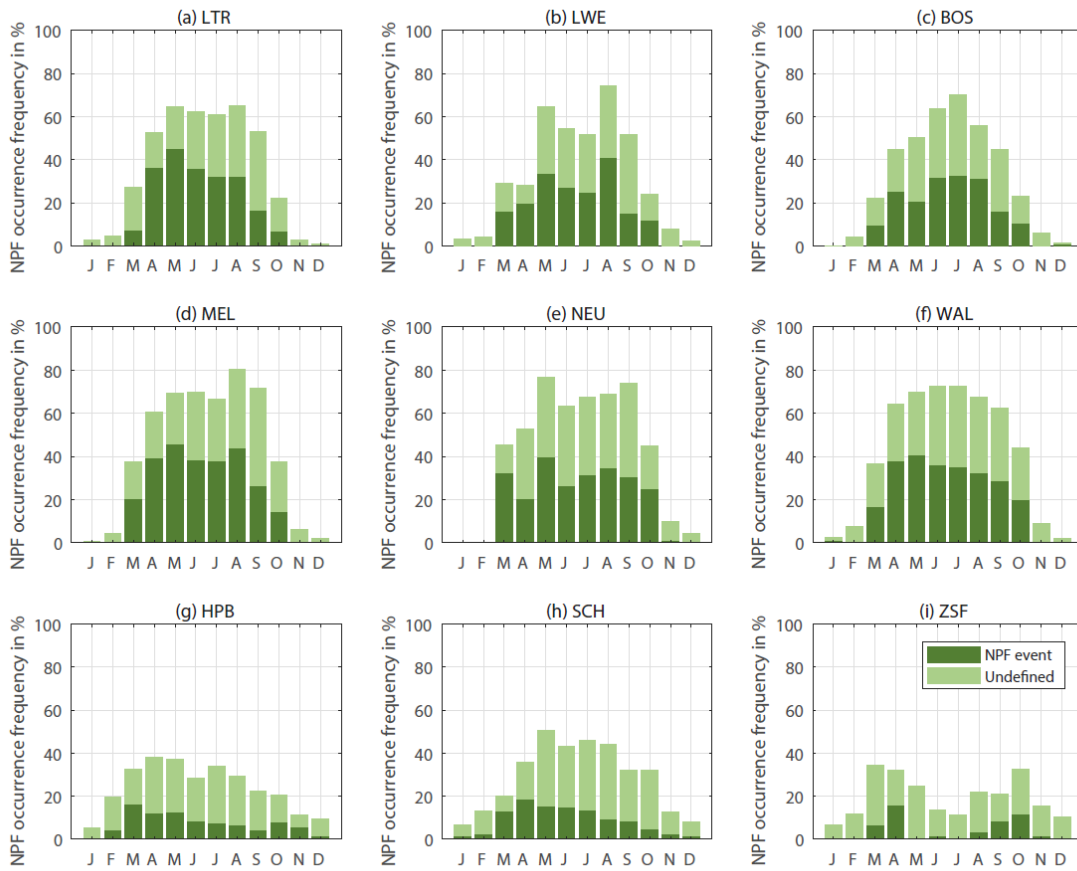
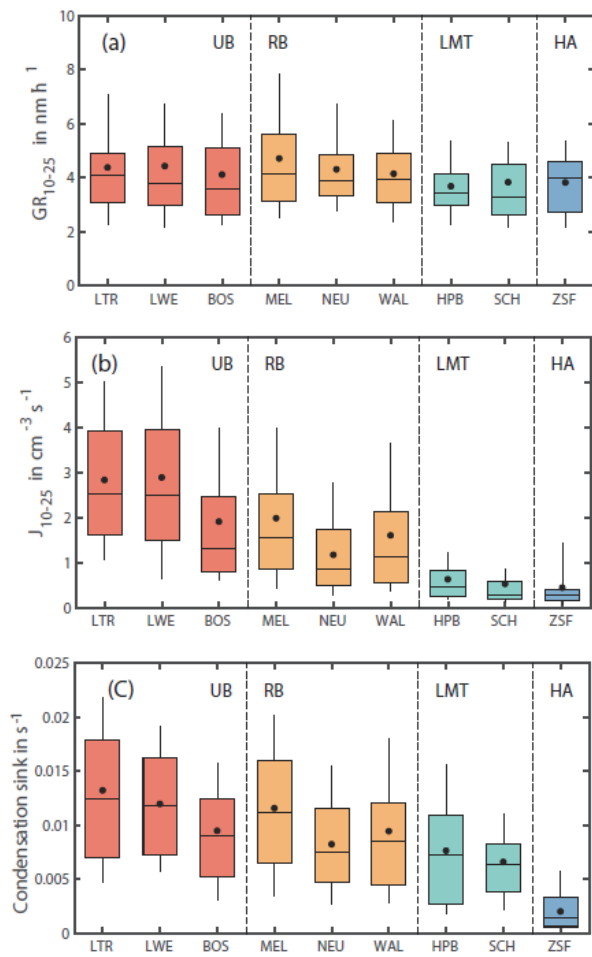
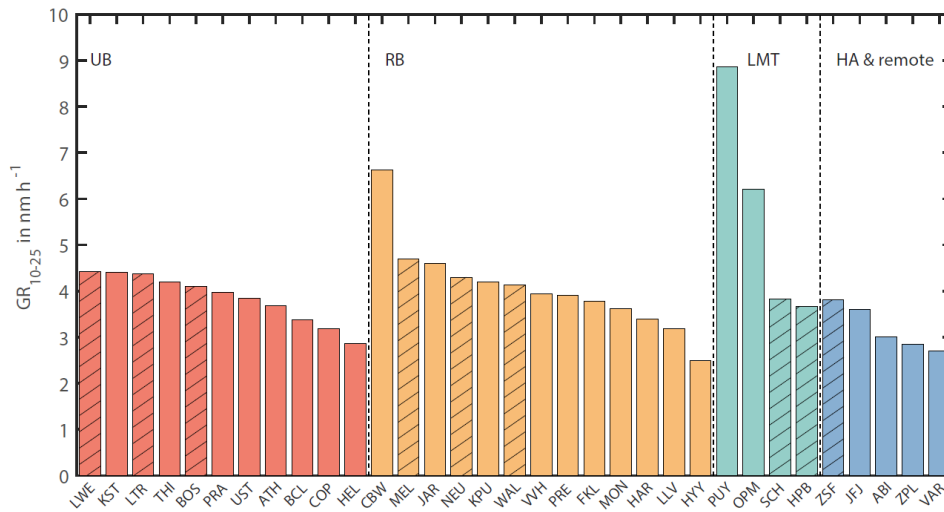


Figure 3: Monthly occurrence frequencies of NPF events for the nine GUAN sites. The dark green bar denotes the occurrence frequencies of the NPF event (class I and II), and light green for the undefined events.



825

Figure 4: Basic statistics of GR_{10-25} , J_{10-25} and condensation sink measured at the GUAN sites. Dots denote the mean values, and the boxes and whiskers denote the 10th, 25th, 50th, 75th, and 90th percentiles.



830 **Figure 5: Average GR₁₀₋₂₅ in the present study and other studies in Europe. The hatched pattern denotes the results for the GUAN sites in this study.**

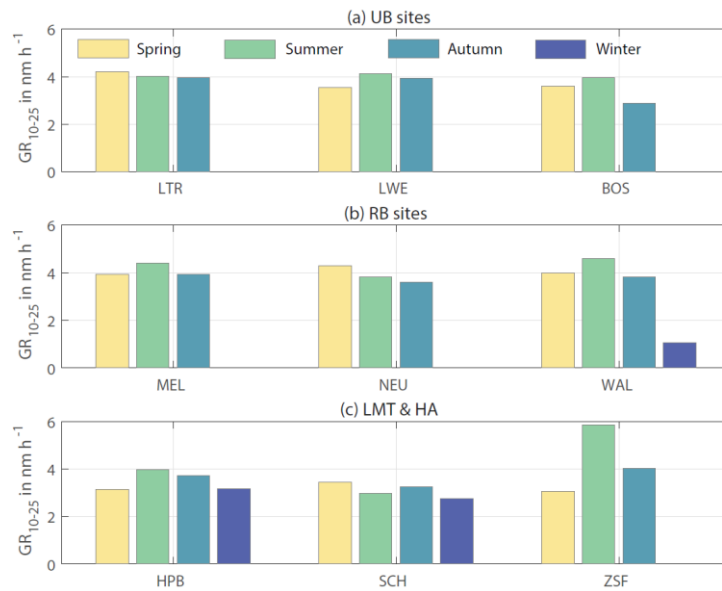


Figure 6: Seasonal mean GR₁₀₋₂₅ of NPF events for the nine GUAN sites.

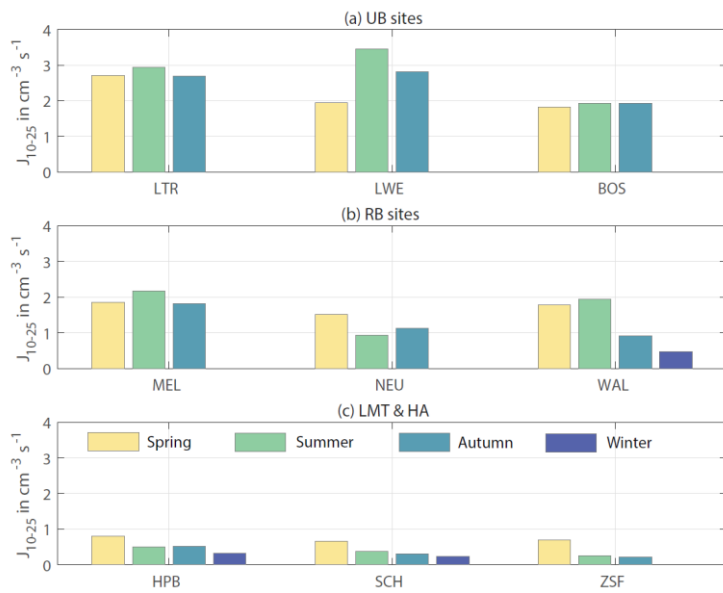


Figure 7: Seasonal mean J_{10-25} for NPF events at the nine GUAN sites.

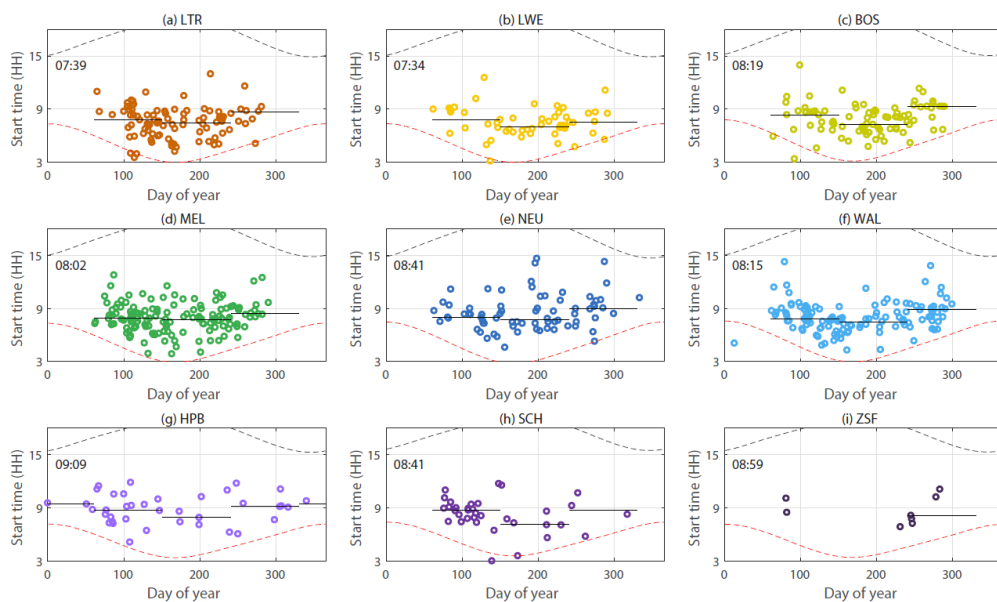
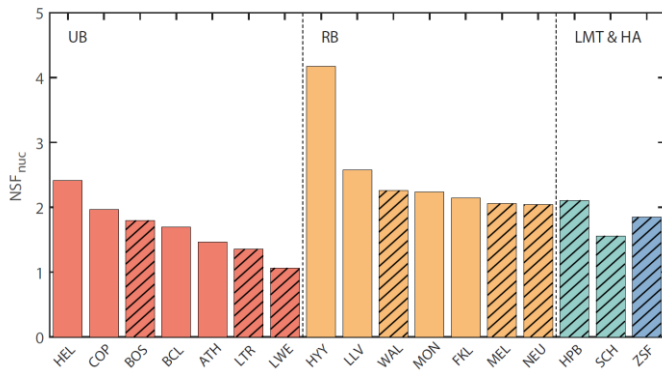


Figure 8: Scatter plot of NPF starting time (solar time) on different days of year. Black solid lines denote the mean seasonal starting time, the red and black dash line indicate the sunrise and sunset time, respectively.



840 **Figure 9: Median NSF in the present study and other studies in Europe. The hatched pattern denotes the results for the GUAN sites in this study.**

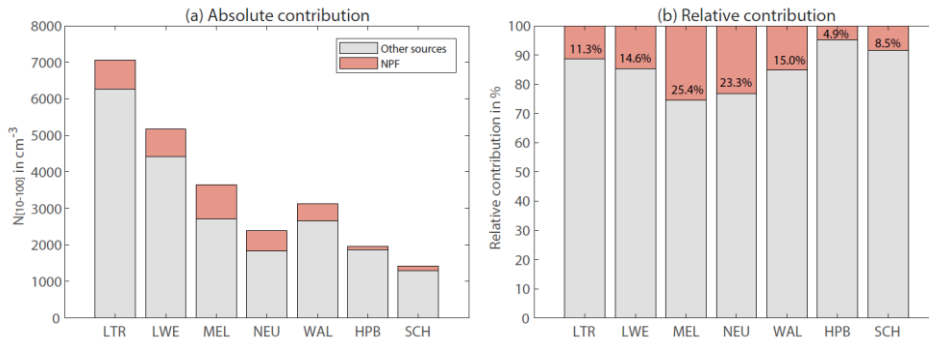


Figure 10: The absolute and relative contribution of NPF (red) on UFP (N_{10-100}) for GUAN sites.

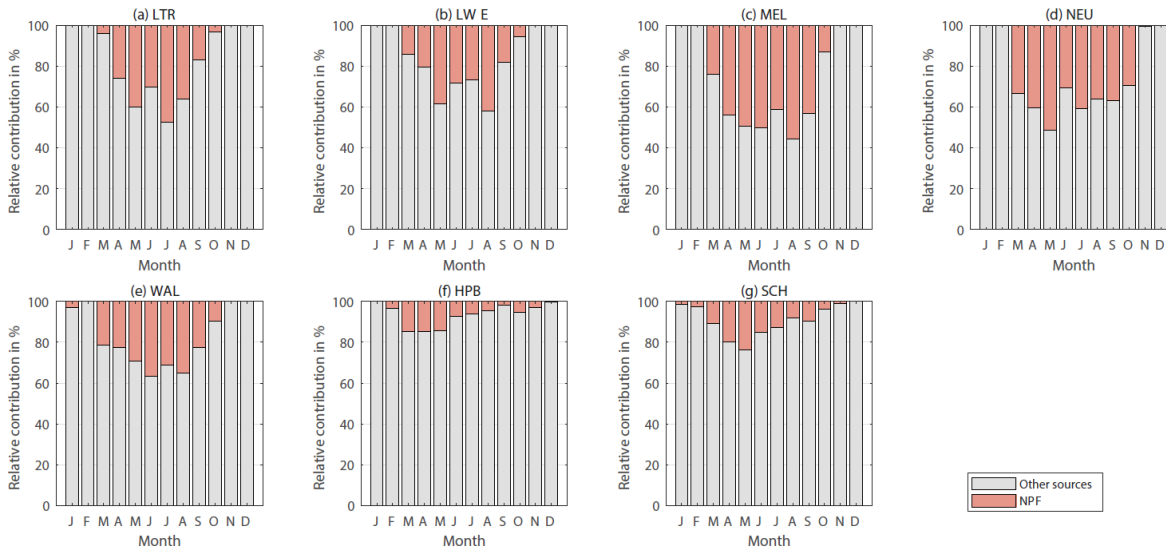


Figure 11: The monthly distribution of relative contribution of NPF on UFP (N_{10-100}) in the seven GUAN sites.

Table 1: Information of the nine GUAN sites and the corresponding PNSD measurements, in alphabetic order.

No.	Site name	Abbrevia- tion	Site category	Altitude	Location	MPSS type	Size range
1	Bösel	BOS	Urban background	17 m	52°59'53" N, 07°56'34" E	MPSS	10–800 nm
2	Hohenpeißen- berg	HPB	Low mountain range	980 m	47°48'06" N, 11°00'34" E	MPSS	10–800 nm
3	Leipzig- TROPOS	LTR	Urban background	126 m	51°21'10" N, 12°26'03" E	TDMPSS	5–800 nm
4	Leipzig-West	LWE	Urban background	122 m	51°19'05" N, 12°17'51" E	TDMPSS	10–800 nm
5	Melpitz	MEL	Regional background	86 m	51°31'32" N, 12°55'40" E	D-MPSS	5–800 nm
6	Neuglobsow	NEU	Regional background	70 m	53°08'28" N, 13°01'52" E	MPSS	10–800 nm
7	Schauinsland	SCH	Low mountain range	1205 m	47°54'49" N, 07°54'29" E	MPSS	10–800 nm
8	Waldhof	WAL	Regional background	75 m	52°48'04" N, 10°45'23" E	MPSS	10–800 nm
9	Zugspitze Schneeferner- haus	ZSF	High Alpine	2670 m	47°25'00" N, 10°58'47" E	MPSS (TSI 3936)	20–600 nm

850 Table 2: Annual occurrence frequency, average growth and formation rates of NPF events at each observation site.

Site category	Site name	NPF occurrence frequency	Undefined event occurrence frequency	GR ₁₀₋₂₅ in nm h ⁻¹	J ₁₀₋₂₅ in cm ⁻³ s ⁻¹
Urban background (UB)	LTR	16.8 %	15.7 %	4.4	2.8
	LWE	15.5 %	14.5 %	4.4	2.9
	BOS	12.6 %	14.6 %	4.1	1.9
Regional background (RB)	MEL	19.6 %	16.9 %	4.7	2.0
	NEU	18.3 %	20.6 %	4.3	1.2
	WAL	19.0 %	19.9 %	4.1	1.6
Low mountain range (LMT)	HPB	6.8 %	15.4 %	3.7	0.6
	SCH	7.8 %	17.3 %	3.8	0.5
High Alpine (HA)	ZSF	3.4 %	14.3 %	3.8	0.4

Table 3: Comparison of the enhancement of CCN by NPF (N_{CCN} enhancement, E_{NCCN}) from multiple European studies.

Site	Site category	Time period	CCN method	Critical diameter in nm	Supersaturation (ss) in %	E_{NCCN}	Reference
LTR, Germany	UB	2009–2013	Calculated	190, 80, 60	0.1, 0.4, 0.6	1.0, 1.3, 1.2	This study
LWE, Germany	UB	2011–2013	Calculated	190, 80, 60	0.1, 0.4, 0.6	1.0, 1.1, 1.2	
BOS, Germany	UB	2009–2013	Calculated	190, 80, 60	0.1, 0.4, 0.6	1.2, 1.6, 1.6	
MEL, Germany	RB	2009–2013	Calculated	190, 80, 60	0.1, 0.4, 0.6	1.1, 1.2, 1.3	
NEU, Germany	RB	2011–2013	Calculated	190, 80, 60	0.1, 0.4, 0.6	1.3, 1.5, 1.5	
WAL, Germany	RB	2009–2013	Calculated	190, 80, 60	0.1, 0.4, 0.6	1.0, 1.2, 1.3	
HPB, Germany	LMT	2009–2013	Calculated	190, 80, 60	0.1, 0.4, 0.6	1.6, 1.7, 1.8	
SCH, Germany	LMT	2009–2013	Calculated	190, 80, 60	0.1, 0.4, 0.6	1.5, 1.8, 1.9	
ZSF, Germany	HA	2012–2013	Calculated	190, 80, 60	0.1, 0.4, 0.6	1.9, 1.8, 1.9	
Vienna, Austria	UB	2014–2015	Measured	57	0.5	1.4	Dameto et al., 2017
University of Crete, Greece	Coastal	2008–2015	Measured	162, 67, 54, 46, 43, 35	0.1, 0.4, 0.5, 0.7, 0.7, 1.0	1.3–1.8	Kalkavouras et al., 2019
Sierra Nevada National Park, Spain	High altitude	2018–2019	Measured	66	0.5	1.8	Rejano et al., 2021
Hyytiälä, Finland	RB	2009–2009	Measured		0.1, 0.2, 0.4, 0.8, 1.0	2.1, 2.1, 1.7, 1.8, 1.7	Sihto et al., 2011
MEL, Germany	RB	May – June, 2008	Calculated	Varied	0.1, 0.4, 0.6	1.6, 1.7, 1.7	Wu et al., 2015
MEL, Germany	RB	May, 2017	Calculated		0.2, 0.4, 0.8	1.0, 1.3, 1.7	Ren et al., 2021
HPB, Germany	LMT	October, 2015	Calculated		0.2, 0.4, 0.8	0.9, 1.1, 1.5	
Vavihill, Sweden	RB	October, 2009	Calculated		0.2, 0.4, 0.8	1.0, 1.2, 1.5	
RV Polarstern, Norway	Polar	June – July, 2018	Measured		0.1–1.0	between 2 and 5	Kecorius et al., 2019

Table 4: The enhancement of extinction coefficient at 550 nm ($\sigma_{\text{ext},550 \text{ nm}}$) by NPF for GUAN sites. The bold numbers denote the statistically significant results with $\alpha=0.05$.

Site category	Site	$\sigma_{\text{ext},550 \text{ nm}}$ enhancement
UB	LTR	1.0
	LWE	1.0
	BOS	1.2
RB	MEL	1.1
	NEU	1.4
	WAL	1.0
LMT	HPB	1.8
	SCH	1.6
HA	ZSF	1.9

860